Development and Characterization of DNA Origami Nanostructures and their Application as an Aptamer-Mediated Targeted Delivery System

by

Fraser Charles Edward Colquhoun

B.Sc. (Honours), Carleton University, 2019

A thesis submitted to the Faculty of Graduate and Postdoctoral Affairs in partial fulfillment of the requirements for the degree of

Master of Science

in

Chemistry

Carleton University
Ottawa, Ontario

Abstract

The predictable geometries and intermolecular interactions of DNA have led to the development of many arbitrary nanoscale objects, including a class termed DNA origami. DNA origami nanostructure fabrication occurs through the folding of long, single-stranded DNA (ssDNA) using short, single stranded oligonucleotides. DNA origami nanostructures have been of particular interest in the fields of analytical chemistry and medicine because of their controllable molecular self-assembly and the highly addressable nature of DNA. Modifications of DNA origami nanostructures are possible by functionalizing or modifying staple strands to allow for the fabrication of nanostructures with controlled location of included moieties. Detailed herein is the development and characterization of DNA origami nanostructures with site-specific modifications for aptamer-mediated binding of target molecules. Molecular self-assembly is performed by thermal annealing and fabricated objects are purified by centrifugal filtration through molecular weight cut-off membranes. Nanostructures are characterized by agarose gel electrophoresis, UV-Vis quantification, and visualization by atomic force microscopy. Thrombin-binding aptamers, TBA15 and TBA29, were captured to the surface of rectangular DNA origami nanostructures and were incubated with the molecular target, thrombin, to demonstrate the site-specific binding of target molecules. DNA origami nanostructures functionalized with aptamers for specific target recognition bear attractive potential for application in targeted therapies and targeted delivery of molecular payloads.

Acknowledgements

I have to start off with a huge thank you to my supervisor Maria DeRosa! Every year you are reaching new levels of success and accomplishments. You're always so cheerful and optimistic, and always know how to put a positive spin on results, even when they might look terrible! It really has been an honour working with you over the last two years.

To my wife, Caroline: you've been patiently waiting for the day that I'm finally done school, and that time has finally come! You've been so supportive of my work and studies along the way, in any way that you can, and I can't express how grateful and appreciative I am for that. Thank you for keeping me sane for the last two years! Love you!

I'd like to give a heartfelt thumbs down to COVID-19 for causing a pandemic that shut down or hindered significant amounts of research. May we never have to deal with that again!

Fiona and Shahad, I'm grateful for all the teatime and laughs over the last couple of years. That kind of 'therapy' and friendship makes the tough times much brighter.

I have to extend a minor apology to Evan Monk for constantly talking his ear off. I think I asked you way too many questions along the way, some of which may have been only to verify that I was still doing basic math correctly. Other times it was complaining about the way the world is. I do also have to thank you for your help along the way. You're always willing to help others with anything, or pass on your knowledge and experience, as long as that person is at least trying their best.

I will close out this section with a quote from Kurt Vonnegut: “Science is magic that works.” Sometimes it really does feel like science is just performing tricks, especially on the nanoscale since we aren’t able to directly observe many of the results but are able to get nice images after mixing up potions in our witch’s cauldron.

People like to say that I must be very smart when I tell them what I’ve been working on throughout my Master’s, but I think that I just work hard to try and understand the topics I’ve been studying. I hope that at some point in the near future there will be a more mainstream understanding of nanoscience as it is such a cool and interesting field of science with so much potential!

Table of Contents

List of Figures

List of Tables

List of Abbreviations

A - adenine

AFM – atomic force microscopy

C – cytosine

diH_2O – deionized water

DNA – deoxyribonucleic acid

dsDNA – double-stranded deoxyribonucleic acid

ssDNA – single stranded deoxyribonucleic acid

DX – double crossover

EDTA – ethylenediaminetetraacetic acid

FB – folding buffer

G – guanine

kb - kilobase

K_d – Dissociation constant

Mg^{2+} – magnesium

MWCO – molecular weight cut off

PCR - polymerase chain reaction

PEG – polyethylene glycol

SELEX – systematic enhancement of ligands through exponential enrichment

TBA – thrombin-binding aptamer

T - thymine

TBE – TRIS/boric acid/EDTA buffer

TE – Tris-EDTA

TEM – transmission electron microscopy

UV-Vis – Ultraviolet-visible spectrophotometry

Chapter 1: Introduction

1.1 Deoxyribonucleic acid (DNA) crystallography and nanoscale structures

In nature, biological materials are self-assembled by following internal information encoded within the biomaterials. This information is stored within DNA, where the sequences of complementary bases between two strands of DNA encode the genetic information that is read by biological machinery to produce larger complexes.[1,2] Complementary strands pair together with strong affinity and predictable geometry to form the canonical double-helix structure of DNA.[3] For much of the past 50 years, DNA has been thought of only as a sort of genetic code to be broken and analyzed, but in the last 20 years there has been a different vein of research into the use of DNA as building blocks for the development of structures on the nanoscale.

In general, the fabrication of nanoscale objects falls under two overarching categories: top-down, or bottom-up synthesis. Top-down approaches refer to processes that reduce macro or microscale materials down to nanoscale objects or features, whereas the bottom-up approach indicates that atoms or molecules will be brought together to produce larger, ordered nanostructures.[3,4] Fabrication of nanomaterials by the top-down approach can be done by methods such as mechanical milling, etching, or sputtering.[5] These methods require external tools that must have increasing precision as the size of fabricated or synthesized nanomaterials diminish.[4] By contrast, bottom-up approaches include chemical layer deposition, templating, and self-assembly.[5]
Bottom-up assembly of nanostructures using DNA can produce stable, and ordered objects, arrays, and devices.[6]

DNA is a fundamental component of biological material. It encodes the genetic information of all living organisms.[6] Each strand of DNA is made up of many subunits,

called monomers, or nucleotides. A nucleotide is comprised of three components: a 2-deoxy-D-ribose sugar, a phosphate unit, and a nitrogenous base that is connected to the ribose unit through a glycosidic bond (Fig. 1-1).[7]

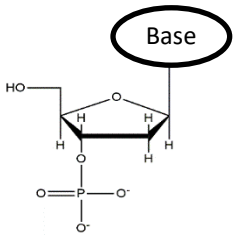

Figure 1-1 Monomer of DNA showing a base that is bound to a 2-deoxy-D-ribose sugar by a glycosidic linkage. The sugar and attached base are bound to a phosphate which is part of the backbone of much larger chains of these subunits. (Structure drawn with ChemDraw)

Furthermore, DNA strands are formed by linking nucleotides together through phosphodiester bonds between the phosphate subunit of one nucleotide and the deoxyribose of the proceeding nucleotide.[7]

DNA is highly stable with a high fidelity of recognition between nucleotides. The four nitrogenous bases that make up DNA sequences are two purines – adenine (A) and guanine (G), and two pyrimidines – thymine (T) and cytosine (C) (Fig. 1-2).

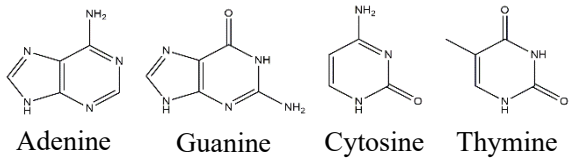

Figure 1-2. The four bases that make up DNA; two purines: adenine and guanine, and two pyrimidines: cytosine and thymine. (Structures drawn with ChemDraw)

While Each base has the ability to interact with every other base, including itself, by hydrogen bonding. Watson-Crick pairing of the complementary purine-pyrimidine base pairs, A-T and C-G, are the favoured types of interactions between oligonucleotides

largely due to their geometrically and energetically favoured hydrogen bonding interactions (Fig. 1-3).[8,9] Pyrimidine-pyrimidine base pairing is unfavourable because the distance between bases is too large for hydrogen bonding to occur. Similarly, purine-purine base pairing is also unfavourable since the bases are too close together, leading to repulsion effects.[9] The arrangements of bases, or the sequence, in the strands of DNA are what encodes the genetic information.[6] The specific pairing relationship between complementary pairs, in conjunction with the geometry of the phosphate and deoxyribose backbone, are what produce the canonical double-helix structure of DNA.

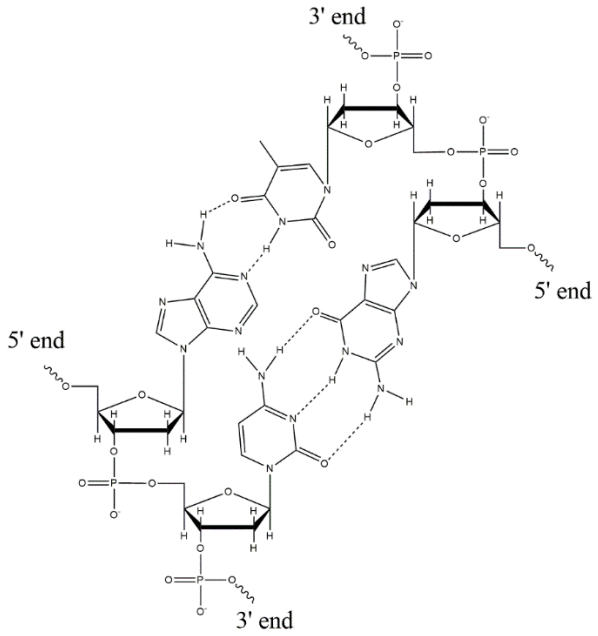

Figure 1-3. Complementarity between bases (A-T and C-G) to form double-stranded DNA. The lower DNA strand has sequence 5'-AC-3', and the upper strand is complementary to the lower strand with sequence of 5'-GT-3'. Complementary bases on opposing DNA strands form hydrogen bonds with each other, giving the DNA its rigidity. (Structure drawn with ChemDraw)

Some DNA may contain discontinuous complementarity, where a short section of the 5' end of one strand overhangs the 3' end of the opposite strand, or vice versa¸

leaving part of the DNA single stranded. These overhangs are termed 'sticky ends' (Fig. 1-4A) as the single-stranded overhang is able to bind to another strand of DNA that is complementary to the sticky end overhang.[2,6] This concept led the initial endeavors of DNA nanotechnology through the 1980s and 1990s that saw the development of self-assembly of two-dimensional (Fig. 1-4B) and three-dimensional lattices comprised of branched junctions.[10]

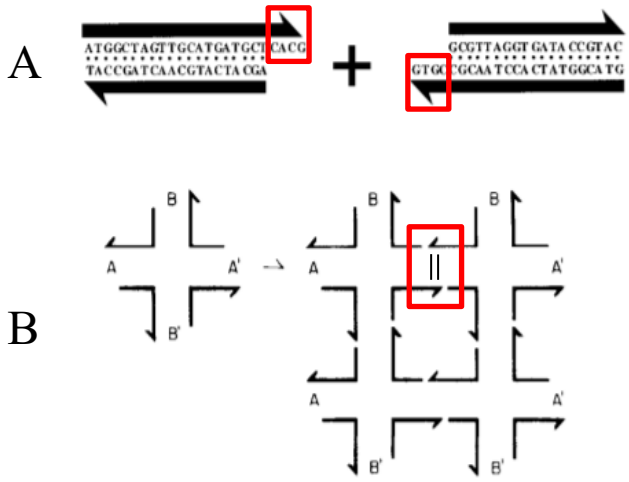

Figure 1-4. A) Illustration of two dsDNA with complementary sticky ends (red boxes). These sticky ends can interact with other ssDNA and bind to their complementary sequence. [adapted with permission from ref.[6]] B) 2D lattice is formed by the joining of complementary bases between sticky ends of the branched junctions (outlined by red box). [adapted with permission from ref.[2]]

Early objectives of DNA nanotechnology were to organize components of nanoelectronics and to crystallize biological macromolecules for crystallography by using DNA as a scaffolding network.[3] Periodic networks were assembled using DNA branched junctions (Fig. 1-4B) linked together by the base pairing of the sticky-end overhangs.[4] The first branched junction networks lacked the stability and rigidity required for use as the building blocks for lattices. To overcome this, double-crossover (DX) molecules were developed. DX molecules are comprised of two double helices fused together by two

strand exchanges.[3,4] In these strand exchanges, a DNA strand will start on one helix and will cross over to the second helix. These DX molecules, or tiles, became the building blocks of DNA crystals. Although DX tiles are also connected by sticky ends, like the branched junctions were, they bore improved rigidity and stability and were used to construct larger 2D and 3D DNA structures with controllable geometry and connectivity.[4]

The predictable geometries and intermolecular interactions of DNA are what make it an attractive material for the fabrication of nanostructures.[11,12] These properties, coupled with advancements in the synthesis of DNA by solid-phase synthesis[13], accelerated DNA nanotechnology research, leading to the development of larger DNA nanostructures.[14–16] Development of these larger nanostructures, and specifically the spontaneous folding of long single strands (1.7kb) into nanoscale octahedron[17], directly led to the introduction of a one-pot synthesis method of synthesizing large DNA nanostructures by sequential folding of a long ssDNA (>7,000 nt) using short complementary ssDNA.[18] The large DNA nanostructures produced by this method are termed DNA origami and have been the focus of significant research over the last 15 years since their introduction.

1.2 DNA origami

First introduced by Rothemund in 2006, DNA origami is dubbed so because it is a process analogous to producing paper origami, which is the art of folding a sheet of paper into arbitrary two- and three-dimensional objects. DNA origami nanostructures are produced in a one-pot synthesis method involving the combination of long, single stranded DNA scaffold and many short oligonucleotides, called staple strands, and slowly annealing the reaction mixture (Fig. 1-5).[18]

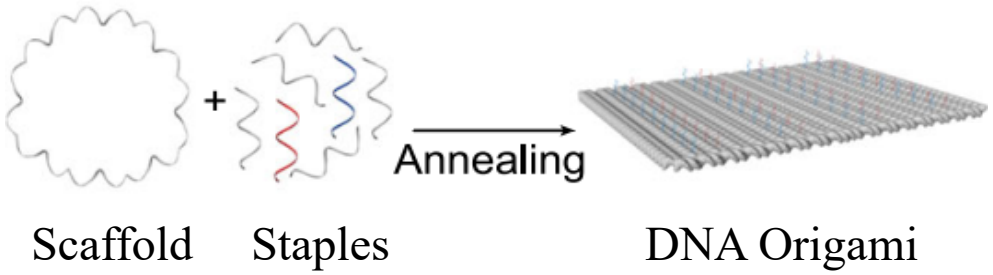

Figure 1-5. Schematic demonstrating a generalized view of DNA origami nanostructure fabrication. [adapted with permission from ref.[19]]

The long ssDNA scaffold strand is frequently a 7,249 nucleotide long single-stranded circular genomic DNA from the virus M13mp18.[18] The folding of this long ssDNA scaffold requires the short ssDNA staples that are complementary to sections of the scaffold strand. Folding of a scaffold strand >7,000 nucleotides in length can require upwards of 200 staple strands, ranging in lengths from 15 to 60 nucleotides.[20,21]

In the process of the folding reactions, the reaction mixtures are heated to high temperatures (~90°C) to denature scaffold and staple strands prior to annealing. As the reaction mixtures are slowly cooled during the annealing process, the staples begin to hybridize to their complementary sequence on the scaffold strand (Fig 1-6).[22] Similar to how DX tiles are more stable than simple branched junctions, staple strands will crossover between adjacent passes of the scaffold strand. This, in turn, increases the stability and rigidity of the overall DNA origami nanostructure.[18]

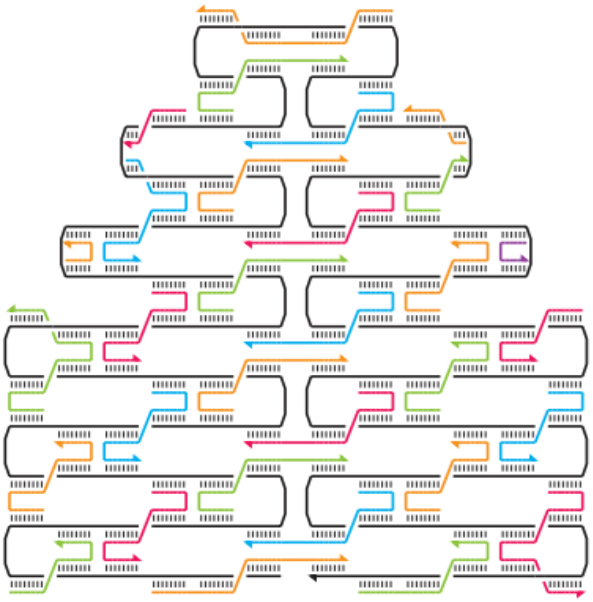

Figure 1-6. Diagram of the folding of a scaffold strand (black) by hybridization of staples (red, orange, green, and blue) to specific regions of the scaffold. [adapted with permission from ref.[18]]

The size of folded DNA origami nanostructures is limited by the length of the scaffold strand. The scaffold may only be folded and twisted a finite number of times through interactions with the staple strands before its entire length is used. In this regard, scaffold strands of custom length may be tailor-made to suit the design requirements of the folded nanostructures. Strategies such as Polymerase Chain Reaction (PCR)-based techniques have been employed to generate custom length scaffold strands. Scaffold strands ranging from 756 to 4808nt in length have been produced through these PCR-based techniques and have been successfully used to produce custom DNA origami nanostructures. Moreover, longer scaffold strands with lengths in excess of 51,000nt have been produced through combinations of site-directed mutagenesis and site- and ligation-independent cloning protocols.[23] Similarly, smaller, minimalistic DNA origami nanostructures in the form of wireframe DNA origami have also been reported.[24–26]

1.2.1 DNA origami design

The original process for the design of DNA origami proposed by Rothemund began with designing and building a model of the desired nanoshape and determining the folding path of the scaffold by hand. Once the shape and folding path had been defined, details of the prepared model could be entered into a computer program as a large set of values containing DNA lengths and offsets of the rows of the scaffold strand in the raster folding patter.[18] This process was found to be tedious and could be prone to errors.

In 2008, Douglas published a free, open-source computer-aided design program by the name 'caDNAno'. The original caDNAno program aided in the design of 3D DNA origami nanostructures (Fig. 1-7) constrained to a honeycomb lattice and made an immediate impact on the design process of DNA origami, eliminating the tedious nature of the hand-built models and reducing any errors incurred from the 'by-hand' design process.[27] Structural parameters such as the distance between antiparallel crossovers, number of base pairs per helical twist, allowable ranges for staple crossovers (e.g. between adjacent scaffold strands, adjacent+1, etc.), and the number of bases required to be hybridized to a scaffold strand before crossover may occur.[27] Modifications to these parameters can be used to reduce mechanical stresses in the overall structure, or to promote the folding of a sheet of DNA origami other nanoshapes.[1,27]

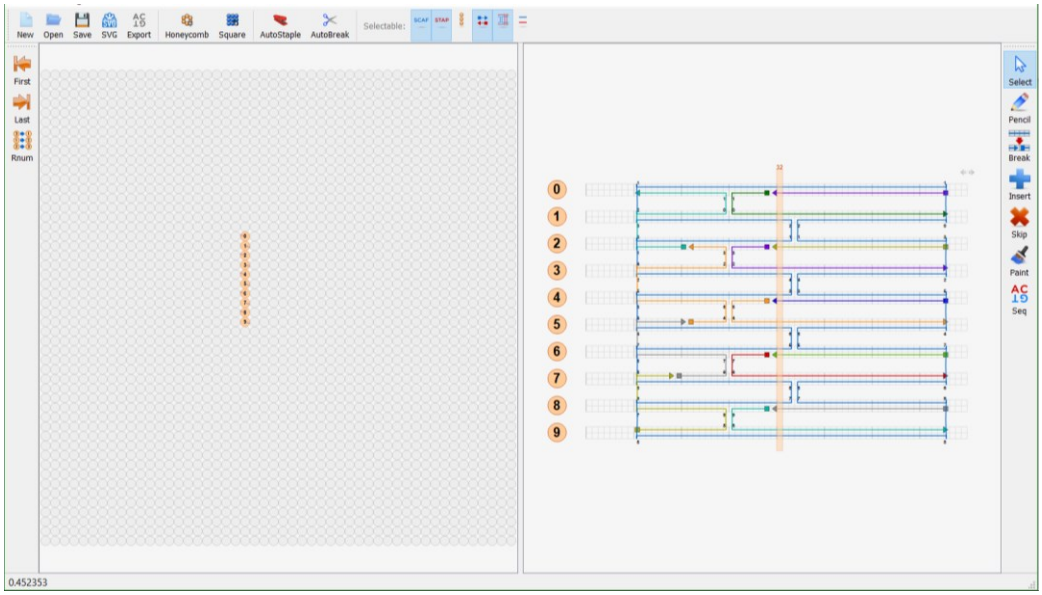

Figure 1-7. Screen capture of the caDNAno2 program, depicting the workspace for the design of a square lattice DNA origami nanoshape. Selection of the lattice shape occurs in the left pane (either square or honeycomb lattice), the scaffold path is manually set in the middle pane, and staples and their sequences are generated automatically.

The caDNAno program became an excellent tool for the design of DNA nanostructures and Castro published an article in 2011 with a step-by-step guide to the design and self-assembly of DNA origami.[20] In their publication, Castro described the design of a nanostructure using caDNAno and introduced a free, web-based computational tool in CanDo. This tool is useful for the prediction of the 3D solution shape and mechanical flexibility (Fig. 1-8) structure of DNA nanostructures.[28] In using CanDo, the double-helix is assumed to be an elastic rod where the base pairs are modeled as two-node beam finite elements. The elastic rod model is given experimentally measured material and geometric parameters such as bending stiffness, axial stretching, length, and diameter. By using this finite element method, highly complex 3D geometries and their flexibility can be predicted when it is not simple to do so analytically. Users

may also specify custom mechanical and geometric parameters for specific DNA origami nanostructure designs.[20]

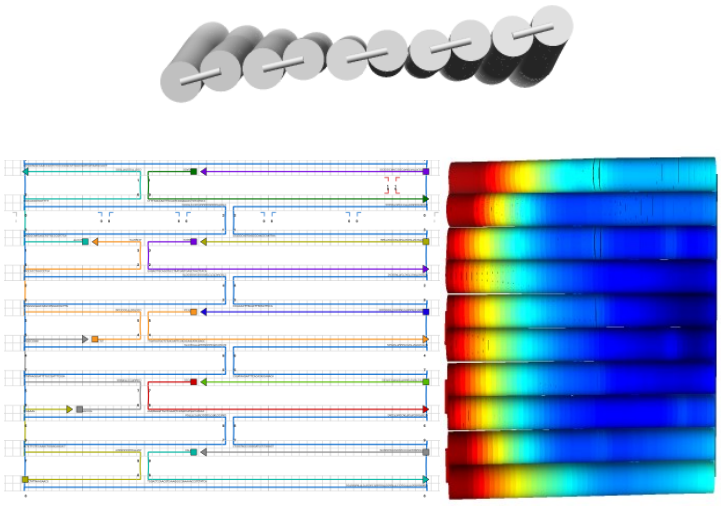

```
Start,End,Sequence,Length,Color
8[30],9[60],TTGTTCCTGGACTCCAACGTCAAAGGGCGAAAAACCGTCTATCA,44,#007200
8[60],8[31],ACTCTAGAGGATCCCCGGGTACCGAGAGTG,30,#1700de
2[16],0[8],ATTGCCCTTCGCCAGGGTGGTTTTTCGGTTTGCGTATTGGG,41,#333333
5[17],2[17],ATCCTGTCGCTGGTTTGCCCCAGCACCGCCTGGCCCTGAACAGCTG,46,#888888
4[60],4[31],CGGAAGCATAAAGTGTAAAGCCTGGGCAAG,30,#7300de
2[30],3[60],ACGGGCAGAGAGTTGCAGGTGCCTAATGAGTGAGCTAACTCACA,44,#333333
7[15],5[16],AATAGCCCGCAAAATCCCTTATAAACAGGCGAAA,34,#b8056c
4[30],5[60],CGGTCCATTGATGGTGGTCTCACAATTCCACACAACATACGAGC,44,#007200
9[8],7[14],CCACTATTAAAGAACGAGTTTGGAACAAGAGTTCAAAAG,39,#57bb00
2[60],2[31],TTAATTGCGTTGCGCTCACTGCCCGCTGAG,30,#7300de
6[30],7[60],AAATCGGAGATAGGGTTGCTCGAATTCGTAATCATGGTCATAGC,44,#007200
0[30],1[60],GGAGAGGCTTTTCACCAGTTTCCAGTCGGGAAACCTGTCGTGCC,44,#f74308
0[60],0[31],AGCTGCATTAATGAATCGGCCAACGCGCGG,30,#cc0000
6[60],6[31],TGTTTCCTGTGTGAAATTGTTATCCGTCCG,30,#f74308
```

Figure 1-8. (Top and right middle, gray) Top and front and views of an example arbitrary rectangular DNA origami 3D shape with high stiffness, as modelled by CanDo (blue to red colouring indicates the amount of out of plane twist of the shape, blue being in plane and darker shades of red being further out of plane). (Left middle) Folding path of a scaffold (light blue) making a rectangle. Staples are shown in various colours. (right) Sequence list for the staples shown on the rectangular structure. Folding path and staple list were generated using caDNAno2.

3D structures and flexibility are modeled by CanDo as thermally induced fluctuations, at room temperature. This is represented by heat maps (Fig. 1-8) with blue colours indicating higher stability, and colours tending towards red indicating less stability and more flexibility.[20]

Other molecular dynamics simulation tools, such as NAMD[29] or GROMACS[30], cannot feasibly be used for DNA origami nanostructure predictions as the size of DNA origami is too large and the miniscule timescales (millisecond to microsecond) for complex events would require an exorbitant amount of computing power.[1] Further updates to the caDNAno software have occurred in recent years from its first iteration published in 2008, and it is now caDNAno v2.5 is available.

Other 3D DNA origami design programs exist, such as 'scadnano.org' which is a web browser-based design tool that has similar functionality to that of caDNAno but allows for more freedom of design, including: base modifications, DNA strand loopouts (Fig. 1-9 A-C) and twist corrections. Including these functions makes it possible to design DNA nanostructures with spatially addressable surface features, such as sticky ends (Fig. 1-9A) or strand loopouts (Fig. 1-9B, C).

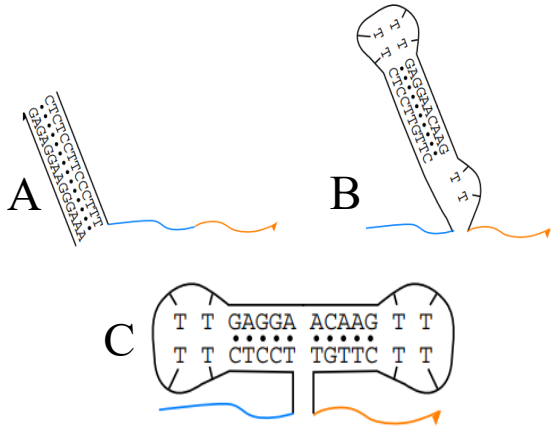

Figure 1-9. Staple strands (blue/orange) with various modifications; A) sticky-ended cohesion of a poly-CT tail, B) loopout where a middle portion of the staple strand is complementary to a proceeding portion of the staple sequence, C) dumbbell-shaped loopout. [adapted with permission from ref.[31]]

There also exists DNA nanostructure computer programs that are meant to design only simple 2D and 3D nanostructures such as wireframe DNA origami.[32] This so-called 2nd generation software[1], was designed to be more user-friendly and require less technical knowledge from the designer. Staple sequences are generated automatically based off user input. These programs include DAEDALUS and TALOS[33] for 3D structures, and vHelix-BSCOR[34], PERDIX[35], and METIS[32] for 2D origami structure design. These design tools may be run through command line prompts, or through MATLAB software.[36] DAEDALUS designed objects (e.g. cubes, pyramids, etc.) are defined through their vertices and an optimal routing path along all edges of the object is determined by an Eulerian circuit method. Optimized routing can occur when the sequence length along all edges is defined in multiples of 10.5bp to satisfy the natural helicity of B-form DNA and to prevent over- and underwinding of DNA.[36,37] The routing procedure is performed and staples sequences are determined according to Watson-Crick complementarity.[36]

DNA origami designed in caDNAno cannot contain both linear and honeycomb lattices. Each design file may only contain one or the other of the two lattice types. The design process is also limited when using caDNAno as DNA double helices must be parallel in design (Fig. 1-7), 3D visualization of designed nanostructures is not feasible, and automated design is not currently possible.[38]

One final design program is Adenita, a 3D interactive toolkit for SAMSON Connect, OneAngstrom's molecular design platform. Adenita is able to overcome the limitations of caDNAno and encompasses elements from the majority of the aforementioned design programs.[1,33] The versatility of Adenita is unsurpassed by any previously reported DNA nanostructure design programs, allowing the user to visualize

structures in fine or coarse detail (Fig. 1-10), manipulate, and create simple DNA structures or combine components to create higher-order structures.

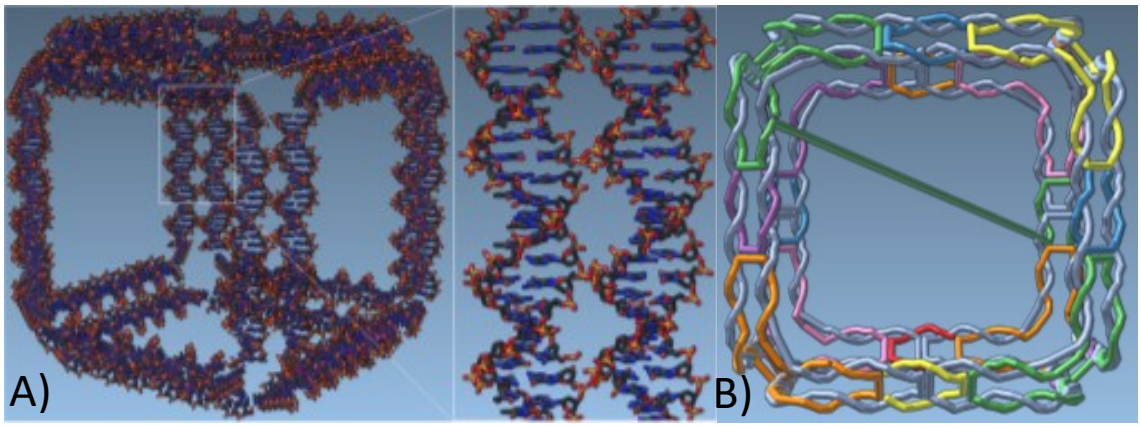

Figure 1-10. Wireframe origami structure visualization levels in Adenita. A) A wireframe cube is visible at the finest scale with the ability to view individual atoms and bonds in the DNA helix. B) Coarse-scale view of the wireframe cube assembly. The scaffold strand is visible in silver-grey, and the staples are assorted colours. [adapted with permission from ref.[39]]

Designs using Adenita can be free form, creating custom raster patterns or incorporating single strands or double helices to existing structures. They can also incorporate wireframe elements using the DAEDALUS algorithm to create parameterizable wirefame structures.[1,33,38] The overall size and specific edge lengths of wireframe structures can be specified and the structures can be modified (Fig. 1-11) or manipulated as desired.

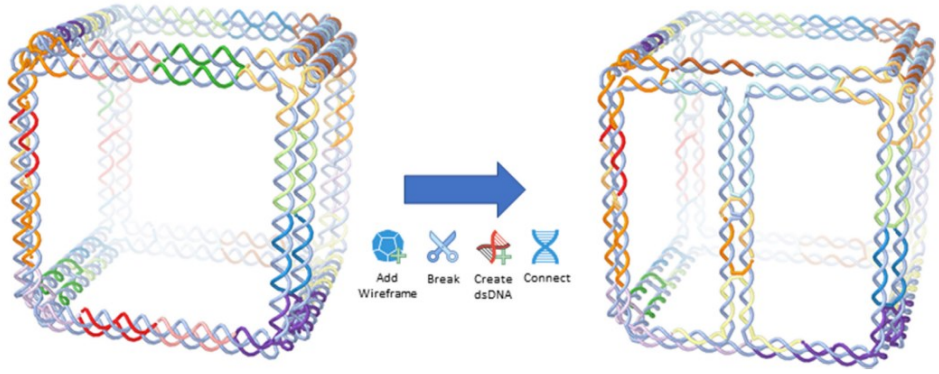

Figure 1-11. Addition of wireframe structure in Adenita, created with the DAEDALUS algorithm and subsequent modification to add an additional edge to the cube. [Adapted with permission from ref.[38]]

caDNAno designs are also able to be imported and manipulated to produce higher-order structures, or to simply introduce modifications, such as sticky-ended staples or staple loopouts (Fig. 1-9). The development of Adenita on the SAMSON Connect platform allows for access to visualization and dynamics simulations and interactions with other systems, including aptamers and proteins.[38]

1.2.2 DNA origami applications

Since the advent of DNA origami in the mid-2000s, there have been significant advancements in the fabrication of nano-sized DNA origami objects and structures, as well as their application towards the fields of templated synthesis, biosensing, and medicine. The versatility of DNA origami has seen the construction of many arbitrary or novelty shapes as proof-of-concept studies, including smiley-faces and stars[18], dolphins with switchable tails[40], and 3D boxes with a controllable lid[41].

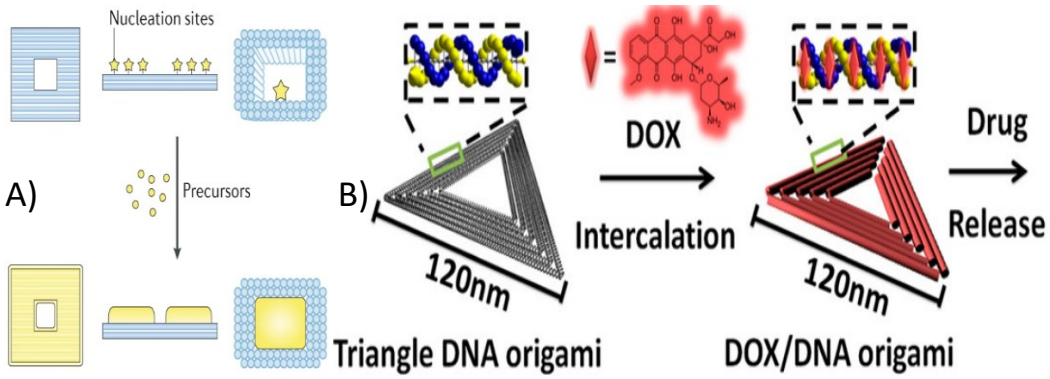

Figure 1-12. A) DNA origami templated synthesis of gold nanomaterials. [adapted from1] B) Triangular DNA origami loaded with doxorubicin, an anti-cancer drug, for targeted delivery. [adapted with permission from ref.[42]]

Further applications of DNA origami nanostructures have been reported for the templated synthesis of gold nanomaterials (Fig. 1-12A)[43], where a DNA origami nanomold is constructed that encloses a gold nucleation 'seed' which grows to fill the nanomold, leaving a gold nanostructure that replicates the cavity. Targeted therapies are another application for DNA origami nanostructures. In these targeted therapies, DNA origami nanostructures are loaded with a drug, or payload, which is delivered to a specific target (Fig. 1-12B)[42,44] either by passive targeting or by active targeting using targeting moieties such as aptamers.[45]

1.3 Aptamers

Aptamers are short, single-stranded oligonucleotides that are highly specific to a target molecule and bind with high affinity.[46] They are selected for specific targets through the Systematic Evolution of Ligands by EXponential enrichment (SELEX), an *in vitro* process involving iterative cycles of selection of a library of random nucleic acids against a specific target.[47] Following selection, aptamers are synthesized through an automated solid-phase synthesis.[48,49] Site-specific modification of aptamers is also

possible during chemical synthesis.[50]Aptamers have been selected for many non-nucleic acid targets including small molecules[51], drugs[52], proteins[53,54], and whole cells.[47]

Aptamers have been reported as being preferentially employed for target recognition over antibodies in certain applications.[50] They have been shown to have equal or superior specificity and affinity for the target of interest than antibodies.[55] The advantages of aptamers over antibodies as molecular recognition tools are also numerous. Aptamers can be developed *in vitro*, with great control over selection parameters, whereas antibodies must be developed *in vivo*.[56]

Aptamers have also been used in a wide range of applications in the fields of analytical chemistry, microbiology, and medicine.[57] A promising application of DNA aptamers lies in their use as a targeting system for delivery of drugs or imaging moieties.[49] High-sensitivity detection of metastatic breast cancer cells was reported using aptamers developed for proteins that are overexpressed on the surface of breast cancer cells.[58] Furthermore, aptamers have been previously developed for thrombin[59,60] and have been used in targeted therapy applications with DNA origami nanostructures.[19]

1.3.1 Thrombin

Thrombin is a serine protease that plays a major role in hemostasis, having both procoagulant and anticoagulant functions.[61] The equilibrium of between bleeding and thrombosis in hemostasis is maintained by thrombin activity, which is part of a feedback loop leading to the formation and regulation of clotting. In the absence of thrombin, fibrinogen cannot be converted to the insoluble fibrin for the formation of clots.[61,62] Conversely, unregulated thrombin activity can cause excessive clotting, resulting in thrombosis, which could lead to cardiovascular disorders such as heart attack or stroke.[62]

Medical treatments for patients with thrombotic disorders must be able to provide rapid and robust antithrombotic treatments that can regulate thrombin activity, preventing thrombosis but not causing excessive bleeding.[61] Anticoagulant drugs, such as low molecular weight heparin and warfarin, are used in hemodialysis to prevent clotting in the extracorporeal circuit. Heparin-like compounds are widely used, but still produce undesirable side effects, including bleeding and heparin-induced thrombocytopenia.[19,63] Post-dialysis treatment bleeding remains a major concern due to the a lack of antidotes able to reverse the anticoagulation effects of heparin-like compounds.[19]

Thrombin activity can be inhibited through the use of direct thrombin inhibitors which can block enzymatic activity by blocking substrate binding at exosites I and II (Fig. 1-13).[53] Both exosites are directly related to the regulation of clotting, as the purpose of exosite I is to aid in the conversion of fibrinogen to fibrin and exosite II is the heparin binding exosite and is important for platelet interactions with thrombin.[53,61]

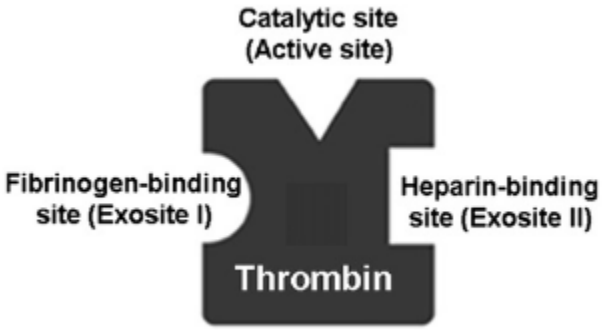

Figure 1-13. Illustration of the binding sites of thrombin and their role in hemostasis. [Adapted with permission from ref.[61]]

While some thrombin inhibitors may be potent inhibitors and have reversible anticoagulation effects they come with adverse side effects and may have narrow therapeutic windows.[53,64] Aptamers capable of binding thrombin have been investigated

as alternatives to thrombin inhibitors currently in use as they are superior in terms of size, produce virtually no immune response[65], are more stable at wide ranges of pH (~4-9), and their anticoagulant activity can be easily controlled by the addition of complementary strands.[61,64]

1.4 Objectives of this Thesis

The objective of this thesis is to contribute to the field of DNA origami through the application of aptamer-mediated target binding to DNA origami nanostructures. First, DNA origami nanostructures will be fabricated, with consideration towards the concentration of magnesium ions in the folding buffer during the thermal annealing process of the folding reactions. Next, the fabricated nanostructures will be purified and characterized by agarose gel electrophoresis (AGE), Ultraviolet-Visible (UV-Vis) spectrophotometry and AFM imaging. DNA origami nanostructures with aptamers hybridized to their surface will be used for target recognition and binding. In addition, alternative methods of purification and characterization will be described. Finally, further applications of DNA origami nanostructures involving target recognition and release will be discussed.

Chapter 2:

DNA origami synthesis and characterization

2.1 Statement of Contributions:

All work described herein was performed by Fraser Colquhoun. AFM imaging of samples by was performed by Dr. Anatoli Ianoul. AFM image analysis was performed by Dr. Anatoli Ianoul and by Fraser Colquhoun.

2.2 Introduction

2.2.1 DNA origami nanostructure synthesis

The fabrication of DNA origami nanostructures is conducted in a one-pot synthesis. Single-layer DNA origami fabrication is possible within a few hours with a high yield, but the folding of larger origami or multi-layered objects can require several days to a week and may only produce a very low yield (<20%).[20] Fabrication begins with the synthesis of short staple strands (15-60 nt) by solid-phase synthesis[13], and the production of the scaffold strand (7249 nt) from viral M13mp18.[18] With large numbers of staples required for the folding of DNA origami nanostructures, the synthesis, purification, and quantification of each of these oligonucleotides would require astronomical amounts of time occupying research lab DNA synthesizers. For this reason, staples used for DNA origami folding reactions were purchased from oligonucleotide manufacturing companies.

Staples and scaffold strands are mixed into one reaction vessel (typically at a molar ratio of 5:1 of staples to scaffold) in a folding buffer containing magnesium salts. Most protocols employ a magnesium concentration near 12.5mM Mg^{2+}. While higher concentrations might be required for larger structures or 3D shapes, assembled DNA origami nanostructures in solutions with high concentrations of Mg^{2+} may be unstable and deteriorate when transferred to solutions with lower salt concentrations.[1] This can be

challenging for biological applications as cellular concentrations of Mg^{2+} can range from 5 to 30mM, and free Mg^{2+} concentrations can be found as low as 0.4mM.[66]

Folding mixtures are then thermally annealed, slowly, at a constant cooling rate. Different origami folding protocols have been reported[19,67,68], each with their own respective thermal annealing program. Some programs initially heat the folding mixtures to temperatures of 90-95°C[19] for 5 minutes before ramping down the temperature at a very slow rate of 0.1°C /minute (1°C/10 minutes), while others perform a longer incubation (15 minutes) at lower temperatures of 60-65°C[67] before decreasing the reaction temperature at a rate of 1°C/minute.

2.2.2 Characterization of DNA origami nanostructures

Folding reactions are typically performed with a large molar excess of staple strands.[18] Therefore, folded nanostructures typically require purification from excess staple strands, or misfolded structures, that remain in solution if they are to be used for any downstream applications. General DNA or protein purification methods may be destructive for the purification of DNA origami nanostructures due to the use of denaturing agents that could disrupt the folded structure of the origami.[69]

Purification methods that can be applied to DNA origami include polyethylene glycol (PEG) precipitation[70], size-exclusion chromatography[71], and the use of spin-filters[72]. Agarose gel electrophoresis (AGE) is a method that is used for the purification of DNA origami[69], but in this work AGE was used solely to visualize the bands of folded nanostructures presenting in the gels. AGE-separated and spin-filter purified reaction mixture bands were visualized in agarose gels and compared to the bands of the 1 kb ladder, scaffold, and staple strands.

Folded DNA origami nanostructures are generally characterized by concentration determination using UV-Vis spectrophotometry and imaging by Transmission Electron Microscopy (TEM) and Atomic Force Microscopy (AFM).[18,20,67,69]

AFM offers visualization and manipulation of nanoscale objects with high resolution.[73] Samples are deposited onto a mica substrate and imaging is performed either in air, or in solution. Samples imaged in air are deposited onto the surface of the mica substrate using a deposition buffer containing divalent cations, such as Zn^{2+}, Ca^{2+}, or Mg^{2+}. These cations mediate the binding of DNA to the substrate by chelating the negatively charged phosphate backbone of DNA and the mica surface.[73,74] Following deposition, the substrate is rinsed to remove residual ions from the deposition buffer. Sample imaging may also be performed in solution but requires functionalization of the mica surface using compounds such as aminopropyl triethoxy silane or silatrane, to provide a positively charged surface for DNA immobilization.[75]

Both contact and non-contact modes can be used for imaging DNA nanostructures. Direct contact modes, where the imaging tip is dragged across the surface of the sample, may be used for manipulation of nanostructures but may displace or distort DNA nanostructures. Intermittent tapping modes offer a solution to these issues as less force is applied to the sample since the tip oscillates above the sample surface and only touches the surface at the bottom of the oscillation cycle. Non-contact tapping modes are also used, where the imaging tip is oscillated above the sample without making contact, detecting tip-surface interactions.[74]

Both of the aforementioned tapping modes are widely used for AFM studies of 1D and 2D DNA nanostructures as they greatly reduce lateral forces on the sample and imaging tip.[74,75]

2.2.3 Aptamers and DNA origami

DNA origami is a highly programmable nanomaterial due to predictable hybridization of the staples to their complement regions on the scaffold strand. Because of this, functional group positioning or target immobilization is possible with nanometer precision.[76,77] This can be accomplished by extending staples to a sequence-dependent 'capture' strand that will protrude from the surface of the origami.[19]

The staple sequences used in this work were based on Zhao's method[19] (assembled according to Rothemund's methods[18], with slight modifications). Modifications between Rothemund's methods and Zhao's methods include the addition of 5T tails to the 5' ends of some edge staples (Table B2) and the exchange of original staple strands for capture strands. The capture strands contain the same sequence as the exchanged strands however, they now possess a 5'-extension of a sticky end that will protrude from the surface of the folded DNA origami. Aptamers TBA15 and TBA29 were also synthesized with an extension to their 5' end that is complementary to the sticky end of the modified staples that will be sticking out from the surface of the origami.[19]

Recently, Zhao, et al. have reported the use of a DNA origami-based nanoarray for the inhibition of thrombin and thrombus formation.[19] DNA origami nanostructures were decorated with two aptamers that had been previously selected for thrombin.

TBA15 and TBA29 (Fig. 2-1) are ssDNA oligonucleotides that have been shown to inhibit thrombin activity.[62]

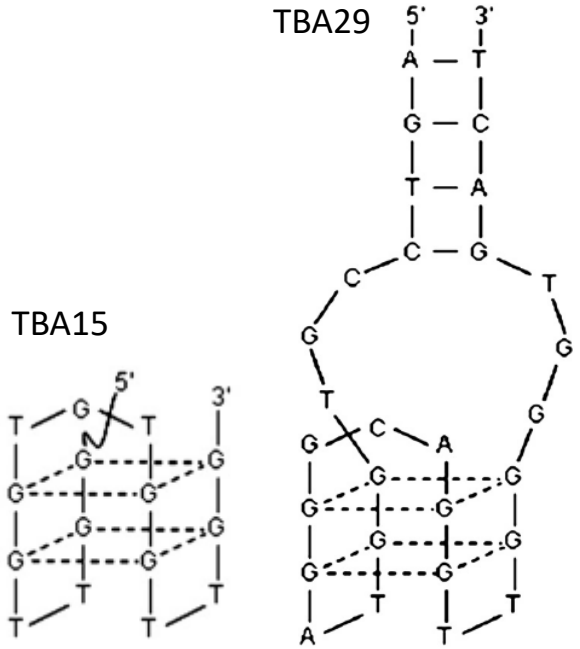

Figure 2-1. Structures of thrombin-binding aptamers TBA15 (left) and TBA29 (right). [adapted from ref.[53,61]]

TBA15 is a 15-nucleotide long aptamer that is able to bind directly to exosite I of thrombin, which is the fibrinogen recognition site. TBA15 (sequence in Table 2-1) can bind to this site with a dissociation constant (K_d) of ~70-100nM and has also been shown to have potent anticoagulant ability.[59] The other aptamer, TBA29 (sequence in Table 2-1) is a 29-nucleotide long aptamer that recognizes thrombin's exosite II – the heparin-binding exosite – with high affinity (K_d ~ 0.5nM).[60]

Table 2-1. Sequences of thrombin recognizing aptamers TBA15[59] and TBA29[60].

Aptamer name	Sequence (5'-3')
TBA15	GGTTGGTGTGGTTGG
TBA29	AGTCCGTGGTAGGGCAGGTTGGGGTGACT

Binding of aptamers TBA15 and TBA29 to the thrombin target was carried out in binding buffers containing either 20mM Tris-acetate, 140mM NaCl, 5mM KCl, 1mM $CaCl_2$, and 1mM $MgCl_2$ (pH 7.4)[59,60] or 50mM Tris-HCl, 100mM NaCl, and 1mM $MgCl_2$ (pH 7.5)– both at 37°C for 5 minutes.[60]

2.2.4 Chapter objectives

The work described herein investigates the potential for the use of DNA origami nanostructures in targeted delivery applications. A magnesium screen will be performed first to determine the optimal Mg^{2+} concentration in the folding reactions, as it is known that the stability of folded origami nanostructures is influenced by the concentration of Mg^{2+} in solution. DNA origami nanostructures will be produced by thermal annealing of folding reaction mixtures (Fig. 2-2). The temperature program of the annealing process will heat reaction mixtures to 95°C for 5 minutes to allow all DNA from the scaffold and staple solutions to denature and ensure all DNA is in its single-stranded form. Annealing of the reaction mixtures will follow this denaturation step. Folded structures will be characterized by AGE, UV-Vis spectrophotometry, and AFM imaging.

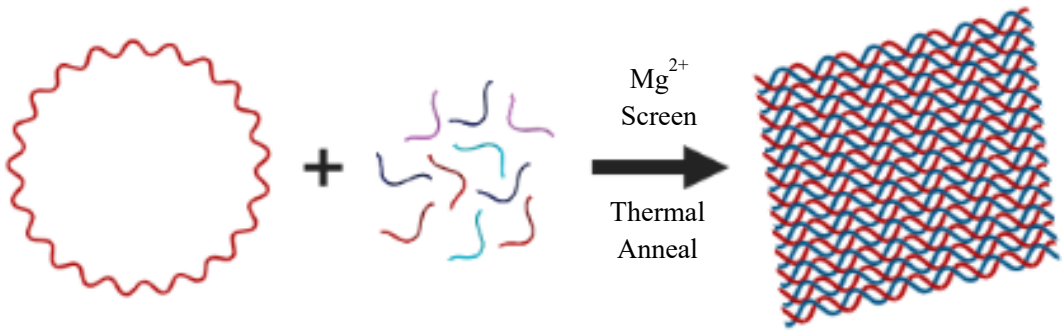

Figure 2-2. Illustration of the initial folding reaction and magnesium screen to fabricate rectangular DNA origami nanostructures. The scaffold strand (red ring) is annealed with many staple strands (multiple colours) in the presence of varying [Mg^{2+}] to determine optimal folding reaction conditions. [Created with BioRender.com]

Select staple strands will be exchanged for aptamer capture staple strands. These capture strands will bear the same sequences as the strands for which they were exchanged but will possess a poly-A or poly-ATA extension that will be complementary to extensions added to aptamers (Fig. 2-3A).

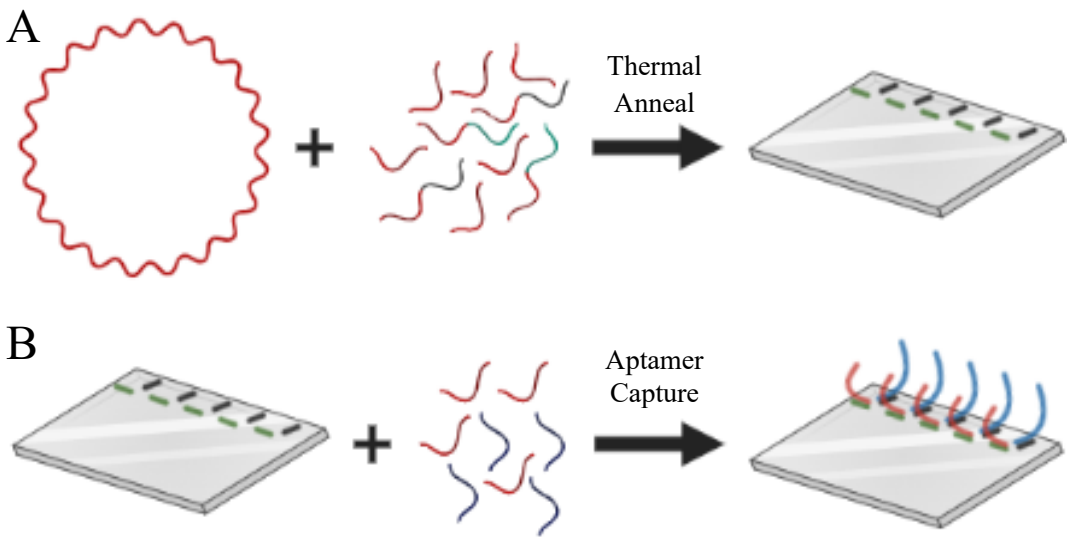

Figure 2-3. Illustrations of A) the folding of rectangular DNA origami nanostructures with capture staples included in its structure, B) hybridization of aptamers to capture sequences extended from staples in the surface of the nanostructures. [Created with BioRender.com]

Aptamers TBA15 and TBA29, previously selected for thrombin, will be captured to the surface of the DNA origami nanostructures through hybridization of their extensions with the extensions of the exchanged staple strands (Fig. 2-3B). Finally, binding of thrombin to the aptamers captured to the surface of the DNA origami nanostructures will be investigated and characterized (Fig. 2-4).

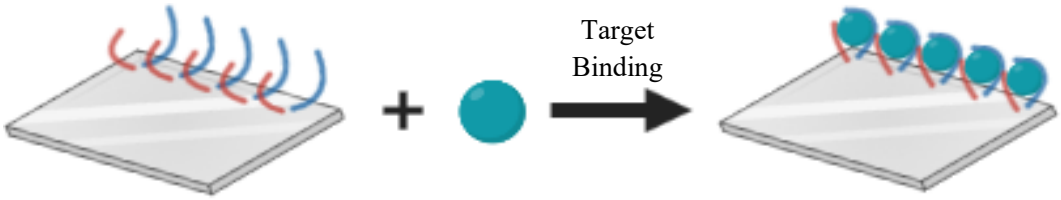

Figure 2-4. Illustration of the target binding to aptamers captured to the surface of the rectangular DNA origami nanostructures. [Created with BioRender.com]

2.3 Methods

All buffer solutions were prepared using deionized water (diH_2O). Boric acid, tris(hydroxymethyl)aminomethane, ethylenediaminetetraacetic acid, sodium chloride, and magnesium chloride hexahydrate were purchased from Bioshop Canada (Burlington, Ontario). A 100nM stock solution of the single-stranded scaffold DNA (type p7249, M13mp18) was purchased from Tilibit Nanosystems (Munich, Germany).

2.3.1 Folding Reactions

A folding buffer (FB) was prepared by dissolving tris(hydroxymethyl)aminomethane (0.9090g, 50mM), sodium chloride (0.4362g, 50mM), and ethylenediaminetetraacetic acid (0.5580g, 10mM) in 150mL of diH2O. The buffer was filtered through a 0.22µm cellulose acetate sterilizing filter and the pH was adjusted to pH 8.0.

Folding reaction mixtures were thermally annealed in an Eppendorf Mastercycler ep Gradient thermal cycler by initially heating the samples to 95°C, holding this temperature for 5 minutes, then cooling to 20°C at a rate of 1°C/min, in steps of 0.1°C. In each folding reaction, staple oligonucleotides were added in a 5:1 ratio with the concentration of scaffold DNA.

2.3.1.1 Initial folding reactions and magnesium screen

Staple oligonucleotides required to form rectangular nanostructure were purchased from Tilibit Nanosystems (Munich, Germany), as a mixture normalized to 400nM of each individual staple, dissolved in ultrapure water.

Folding reaction mixtures were prepared to 50µLvolumes in 0.2mL PCR tubes by combining 10µL of scaffold DNA (20nM), 12.5µL of staple stock (100nM), 22.5µL of diH_2O, and 5µL of FB(X) (Table 2).

A magnesium screen was performed to investigate the effect of magnesium concentration in the folding buffer on the folding of DNA origami nanostructures. Concentrations of magnesium in the folding buffer ranged from 5mM to 30mM, for final concentrations ranging from 0.5 to 3mM in the folding reactions. Six samples were prepared for the magnesium screen, with each sample bearing one of the six folding buffers listed in Table 2-2.

Table 2-2. Concentration of Mg^{2+} in each of the folding buffers tested in the initial Mg^{2+} screen.

FB(X)	$[Mg^{2+}]$ in buffer (mM)	$[Mg^{2+}]$ in folding reaction (mM)
FB(5)	5	0.5
FB(10)	10	1.0
FB(15)	15	1.5
FB(20)	20	2.0
FB(25)	25	2.5
FB(30)	30	3.0

Folding reaction mixtures were thermally annealed, as previously described. From the results of the magnesium screen, it was determined that subsequent folding reactions would be prepared using FB(30), for a final magnesium concentration of 3.0mM in the folding reaction mixtures.

2.3.1.2 Rothemund rectangle

Staple oligonucleotides were purchased from Integrated DNA Technologies (Coralville, IA, USA) in 96-well plates, normalized to a concentration of 100μM of each staple, in 100μL of buffer (10mM Tris/HCl, 0.1mM EDTA, pH 8.0). Stock solutions of staples was prepared by combining the 208 staple strands (Tables 3-1 and 3-2, Appendix B1) in 1250μL, normalizing individual staple concentrations to 400nM.

Folding reaction mixtures were prepared to 50μL volumes in 0.2mL PCR tubes by combining 10μL of scaffold DNA (20nM), 12.5μL of staple stock (100nM), 22.5μL

diH_2O, and 5µL of FB30. Folding reaction mixtures were thermally annealed, as previously described.

2.3.1.3 Rothemund rectangle modified with capture staples

Capture staple oligonucleotides were purchased from Integrated DNA Technologies (Coralville, IA, USA) in 96-well plates, normalized to a concentration of 100µM of each staple, in 100µL of buffer (10mM Tris/HCl, 0.1mM EDTA, pH 8.0). A new stock solution of staples was prepared by combining the 208 staple strands in 1250µL, normalizing individual staple concentrations to 400nM. For this new staple stock, capture staple strands (Tables 3-3 and 3-4, Appendix B1) were substituted into the staple mixture in place of the staples bearing the same staple number (Table 3-1, Appendix B1). For example, capture staple 27-A was added to the staple mixture in place of staple S27.

Folding reaction mixtures were prepared to 50µ, 55µL, or 100µL volumes in 0.2mL PCR tubes by combining volumes of folding reaction components listed in Table 2-3. Folding reaction mixtures were thermally annealed, as previously described.

Table 2-3. Volumes and concentrations of each component of the folding reactions added to the folding reaction PCR tubes. A and B refer to the concentrations of scaffold in the folding reaction, where A = 20nM and B = 40nM.

Sample volume	Scaffold (µL)	Staples (µL)	diH_2O (µL)	FB30 (µL)
50µL (A)	10	12.5	22.5	5
55µL (B)	20	25	---	10
100µL (A)	20	25	45	5
100µL (B)	40	50	---	10

2.3.1.4 Purification of folded DNA origami

Following the completion of the folding reaction, excess staples were removed from solution using Amicon Ultra 0.5mL centrifugal filters Millipore (Sigma Aldrich, Oakville, ON), with a 100kDa filter cut-off. A wash buffer was prepared by dissolving $MgCl_2$ (0.0203g, 10mM) in 10mL of FB.

The entire folding reaction volume (50 or 100µL) was transferred to a 100kDa filter column and was centrifuged at 9,600 x g for 10 minutes. 400µL of the wash buffer was added to the filter column and the sample was centrifuged at 9,600 x g for 10 minutes. This step was repeated once more. For the final wash, 400µL of the wash buffer was added to the filter column and the sample was centrifuged at 9,600 x g for 5 minutes. Finally, the filter column was removed from its wash microcentrifuge tube, then was placed upside down in a clean microcentrifuge tube and centrifuged at 9,600 x g for 1 minute to recover the concentrate. Typically, a final volume of 20-40µL of concentrated

folded origami was recovered. Purified DNA origami samples were characterized by UV-Vis, AGE, and AFM.

2.3.2 Characterization of DNA origami

2.3.2.1 Agarose gel electrophoresis (AGE)

AGE experiments were performed using an Owl™ A1 Large Gel System connected to an E-C Apparatus Corporation EC-105 power supply. Ultrapure agarose powder and SYBR™ Safe DNA Gel Stain were purchased from Invitrogen (Thermo Fisher Scientific, Nepean, ON). 1kb ladder and 6X TriTrack DNA loading dye were purchased from GeneRuler (Thermo Scientific, Nepean, ON).

A stock solution of 5xTBE buffer was prepared by dissolving tris(hydroxymethyl)aminomethane (215.63g, 1.78mol), boric acid (110.06g, 1.78mol), and ethylenediaminetetraacetic acid (14.89g, 0.04mol) in 4L of diH_2O. The buffer was filtered through a 0.22µm cellulose acetate sterilizing filter and the pH was adjusted to pH 8.0. A 0.5xTBE buffer was then prepared by diluting 400mL of the stock 5xTBE buffer in 4L of diH_2O. The running buffer was prepared by dissolving $MgCl_2$ (3.1308g, 11mM) in 1.4L of 0.5xTBE buffer and stirring until completely dissolved. A 1.375M magnesium stock solution was prepared by dissolving 4.1930g of $MgCl_2$ in 15mL of diH_2O.

A 1.0% agarose gel (11.4x13x0.5cm) was prepared by combining 0.75g of ultrapure agarose powder with 78mL of 0.5xTBE buffer, and gently swirling. The agarose-buffer mixture was then heated in a microwave in 30 second intervals, swirling after each heating interval, to dissolve the agarose powder. Once dissolved, the molten agarose mixture was left to cool to approximately 65°C. 8µL of SYBR Safe DNA Gel

Stain and 0.6mL of the 1.375M magnesium stock were added, and the solution was swirled until the red colouring from the addition of the gel stain was evenly dispersed. After further cooling to approximately 55°C, the agarose solution was poured into the gel cast. The well comb was inserted, and the gel was covered and left to solidify for 20-30 minutes. Once the gel had solidified, the running buffer was poured into the buffer chamber, covering the gel. The gel and running buffer were equilibrated for 10 minutes at 120V prior to sample loading.

Samples were prepared for AGE by combining 10µL of sample and 2µL of 6X loading dye in 0.2mL PCR tubes. Samples were gently vortexed and 10µL of each sample-dye mixture was transferred to separate wells in the agarose gel. Gels were electrophoresed at 120V for 2 hours and bands in the gel were imaged at an excitation wavelength of 302nm (at low and high intensity) using an Alpha Innotech AlphaImager EC.

2.3.2.2 UV-Vis Quantification

DNA origami concentrations were quantified using a Varian Cary 300 Bio UV-Visible spectrophotometer. diH_2O or FB(10) were employed as sample diluents and in background cell. After normalizing sample runs at 300nm the absorbance of samples at 260nm was used to calculate an approximate concentration of DNA. Two calculations for determining the concentration of folded DNA origami were used in this work. The first being Equation 1[78]:

(1) $$C_{purified} = \frac{A_{purified}}{A_{unpurified} - A_{staples}} C_{unpurified}$$

Where $C_{purified}$ is the concentration of DNA origami following purification by centrifugation, $A_{purified}$ is the absorbance of the purified DNA origami, $A_{unpurified}$ is the absorbance of the reaction mixture without purification, $C_{unpurified}$ is equal to the initial concentration of the scaffold (typically 20nM), and $A_{staples}$ is the absorbance of a sample containing 4x concentration of the scaffold.

$$C_{purified} = \frac{0.45717}{0.36617 - 0.23006}(20nM) = 67.18nM$$

This concentration was calculated for a purified sample that came from the filtration of 100µL from two separate folding reactions. Dividing this concentration by two will provide the approximate concentration of purified, folded DNA origami from a 100µL folding reaction volume, following the composition of Table 100µL (A).

$$\therefore C_{purified} = \frac{67.18nM}{2} = 33.59nM$$

The second calculation used an approximate extinction coefficient (Equation 2) to calculate the concentration of folded DNA origami through the Beer-Lambert equation (Equation 3)

(2) $$\epsilon_{scaffold} = 68{,}842{,}800 \frac{L}{mol \cdot cm}\left(\frac{50\frac{\mu g}{mL}}{33\frac{\mu g}{mL}}\right)$$

$$\epsilon_{scaffold} = 104{,}307{,}272.2 \frac{L}{mol \cdot cm} = 1.043x10^{8} \frac{L}{mol \cdot cm}$$

The sequence of the scaffold strand (p7249) was entered into the online IDT OligoAnalyzer tool, which returned an extinction coefficient of $\epsilon_{scaffold} = 68{,}842{,}800 \frac{L}{mol \cdot cm}$ (Equation 2). A ratio of the approximate extinction coefficients at 260nm was used to convert the extinction coefficient of the scaffold DNA to that of dsDNA.

dsDNA has approx. OD of 50 µg/mL and ssDNA has approx. OD of 33 µg/mL. Then, the concentration was calculated by the Beer-Lambert equation (3).

(3) $$A = \epsilon c l$$

$$C = \frac{A}{\epsilon l} = \frac{0.45717}{1.043x10^{8} \frac{L}{mol \cdot cm}(1cm)} = 4.38x10^{-9}M$$

This concentration was from a sample diluted for UV-Vis. The undiluted concentration of the purified folded DNA origami was:

(4) $$C_1 V_1 = C_2 V_2$$

$$C_1 = \frac{C_2 V_2}{V_1} = \frac{(100\mu L)(1.4032x10^{-9}M)}{5\mu L} = 28.06nM$$

2.3.2.3 Atomic force microscopy (AFM)

Mica plates for sample deposition were purchased from Ted Pella, Inc. (Redding, CA, USA). The surface of a mica plate was cleaved and 10µL of sample was pipetted to the center of the freshly cleaved mica and left to adsorb for 10 minutes. Sample spots were washed twice by pipetting 50µL of diH_2O onto the spots and allowing them to dry.

Mica plates loaded with adsorbed sample were mounted to square glass slides using Scotch tape and sent for imaging. AFM imaging of DNA origami nanostructures was performed by Dr. Anatoli Ianoul by tapping mode AFM, in air on an NT-MDT Ntegra AFM. A frequency of 67kHz was used for the 10nm radius tip with a spring constant of 0.35N/m.

2.3.3 Aptamer capture

Aptamers T-TBA15 (aptamer TBA15 with a 5' extension) and AT-HD22 (aptamer TBA29 with a 5' extension) were purchased from Integrated DNA Technologies (Coralville, IA, USA). A stock solution for each of T-TBA15 and AT-TBA29 was prepared by diluting 5µL of the 100µM stock solution into 995µL of diH_2O.

Table 2-4. Sequences of modified thrombin-binding aptamers TBA15 and TBA29.[19]

Aptamer	Sequence
T-TBA15	TTT TTT TTT TTT TTT ACGC GGTTGGTGTGGTTGG
AT-TBA29	TAT TAT TAT TAT TAT TTTT AGTCCGTGGTAGGGCAGGTTGGGGTGACT

Purified DNA origami samples were combined with aptamers T-TBA15 and AT-TBA29 at a 3:1 ratio of aptamer to binding site. Aptamer capture solutions were made to 100µL by adding 50µL of purified, folded origami and adding the appropriate volume of aptamers T-TBA15 and AT-TBA29.

Mixtures were heated to 45°C for 5 minutes and then annealed from 45°C to 25°C at a rate of 0.2°C/min, in steps of 0.1°C, for 5 cycles. Excess aptamers were removed by filtering the reaction mixtures through 100kDa centrifuge tubes by the same procedure

described previously. Recovered volumes of purified samples were characterized by UV-Vis, AGE, and AFM.

2.3.4 Binding thrombin to origami-aptamer assembly

Human α-thrombin was purchased from Haematologic Technologies Inc. (Essex Junction, VT, USA) at a size of 1mg in 50% glycerol/water (v/v) at a concentration of 8.0 mg/mL (216.2μM). A stock thrombin solution was made by diluting 11.56μL of thrombin in FB(30), for a final volume of 1mL (2.5 μM).

For the target-binding incubation, thrombin was combined with purified DNA origami at a ratio of 10:1 of thrombin to purified origami. A 100μL reaction volume was prepared by combining 90uL of purified DNA origami (~10nM), 3.5μL of the 2.5 μM thrombin stock (200nM), 6.5μL of FB30. The thrombin-binding reaction mixture was incubated at 25°C for 30 minutes, in the Eppendorf Mastercycler ep Gradient thermal cycler. Samples were characterized by AGE, UV-Vis, and AFM.

2.4 Results and Discussion

2.4.1 Setting up folding reactions

The aim of the initial folding reactions in this work was to make use of a previously prepared staple mixture, ordered from Tilibit Nanosystems, to fabricate and characterize DNA origami nanostructures. This was performed as a method validation to compare experimental results to expected results from literature sources. Once validated, modifications to specific staple sequences could be performed to achieve site-specific addressability for target recognition.

Several published works were consulted in the development of a thermal anneal method for DNA origami folding reactions. The temperature programs from the methods of these publications all varied from one another by either the time of reaction (rate of

thermal ramp down) or their initial denaturing temperatures. Time of reaction for small or single-layered DNA origami nanostructures was found to be typically around 2 hours, while reaction times for larger or multi-layered origami tended to be on the order of hours to days (e.g. 10 hours – 5 days).[18–20,67]

The temperature program in this work began with an initial reaction temperature of 95°C, as heating DNA to this temperature is a common way of denaturing dsDNA.[79] Heating to 95°C and holding this temperature for 5 minutes was done to ensure that all DNA involved in the folding reaction (scaffold and individual staples) were in their single-stranded form.

Annealing of the first two folding reactions was carried out from 95°C to 4°C at a rate of 1°C/minute. This temperature program worked well if folding reaction samples were not going to be immediately used further and were to be stored as folded DNA origami are able to be stored at temperatures below 4°C without suffering from unfolding.[80] However, if samples were to be characterized by AGE or UV-Vis shortly after the folding reaction then the samples would have to be warmed up to room temperature to eliminate any temperature effects, as imaging was performed at room temperature and all buffers and compounds used for these imaging processes were stored also stored at room temperature. It was decided that the temperature program would be altered to maintain the same initial denaturation temperature and rate of cooling, but the ending temperature of the annealing process would be increased to 20°C, a temperature more in line with ambient temperature in the lab. The final temperature program that was used for all subsequent folding reactions is found in Table 2-5.

Table 2-5 Final temperature program for the formation of rectangular DNA origami nanostructures.

Reaction Steps	Description
Step 1	Heat to 95°C
Step 2	Hold 95°C for 5 minutes
Step 3	Cool from 95°C to 20°C @ 1°C/min
Step 4	Hold 20°C indefinitely

2.4.2 Magnesium screen

The next component of the folding reactions that was investigated was the concentration of magnesium (Mg^{2+}) in the folding buffer, and for this a magnesium screen was performed. Screening of folding conditions is useful for determining reaction conditions that will produce efficient self-assembly of DNA origami nanostructures. Performing screens of folding conditions can aid to mitigate side products and optimize fabrication yields.[67] Six folding reactions were tested with increasing concentrations of Mg^{2+} from 0.5mM to 3.0mM. This range of magnesium ion concentration was determined with respect to physiological conditions, which indicate free Mg^{2+} in concentrations of approximately 0.4-0.6mM and cellular Mg^{2+} content ranging from 5-30mM.[66]

Figure 2-5, showing AGE of the first magnesium screen, does appear to show that there is some folded structure. Bands around 2,000bp (indicated by the red arrow, Fig. 2-5) are bands of folded DNA origami. Streaking, or 'smearing', of the bands was observed in all lanes from 0.5 – 3.0, which could be associated with misfolded or partially folded DNA origami nanostructures. Faint, secondary bands around 3,500-4,000bp (indicated by

the white arrow, Fig. 2-5) were also observed in each of lanes 0.5 – 3.0 and could indicate that folded structures may be aggregating, causing them to migrate much slower through the agarose gels.

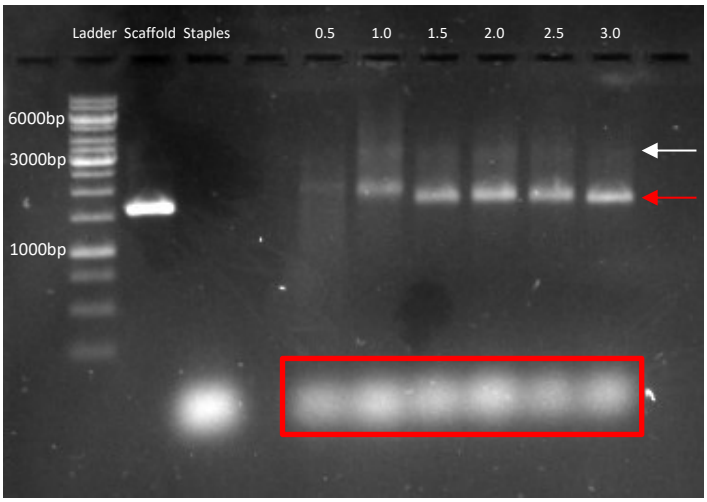

Figure 2-5. AGE image of folding reactions from the first [Mg^{2+}] screen. Lanes numbered 0.5 through 3.0 correspond to folding reactions with increasing [Mg^{2+}] from 0.5 to 3.0mM. The red box indicates the excess staples remaining in the samples following the folding reaction. The red arrow indicates the band of folded DNA origami nanostructures while the white arrow indicates a secondary band.

A dilute folding buffer (0.1xFB – 5.0mM Tris, 5.0mM NaCl, 1.0mM EDTA, pH 8.0) was used for the folding reactions, with varying concentrations of Mg^{2+} ranging from 0.5mM to 3.0mM. While using the dilute folding buffer appeared to show strong folding results across lanes 1.5, 2.0, 2.5, and 3.0 (numbering corresponds to the [Mg^{2+}] in the folding reaction mixture), the original folding buffer (FB – 50mM Tris, 50mM NaCl, 1.0mM EDTA, pH 8.0) was used in proceeding experiments to more closely follow literature folding buffer concentrations.[19]

A second magnesium screen was then performed using the original folding buffer, FB, and the same range of concentrations of Mg^{2+} (0.5mM to 3.0mM). It should be noted

that the bands observed at the bottom of the lanes in both Figure 2-5 and Figure 2-6 (highlighted by red boxes) are from excess staples that were not used in the folding of the DNA origami. There is generally a considerable amount of excess staples visible in AGE images as the molar ratio of staple strands to scaffold strands is 5:1. This would mean that a synthesis with 20nM of scaffold would theoretically only use 20nM of staple strands if the yield were 100%. This would leave 80nM of staples in excess, producing the bright bands at the bottom of the AGE images in each lane. Folding reaction mixtures were purified by spin filtration for later folding reactions.

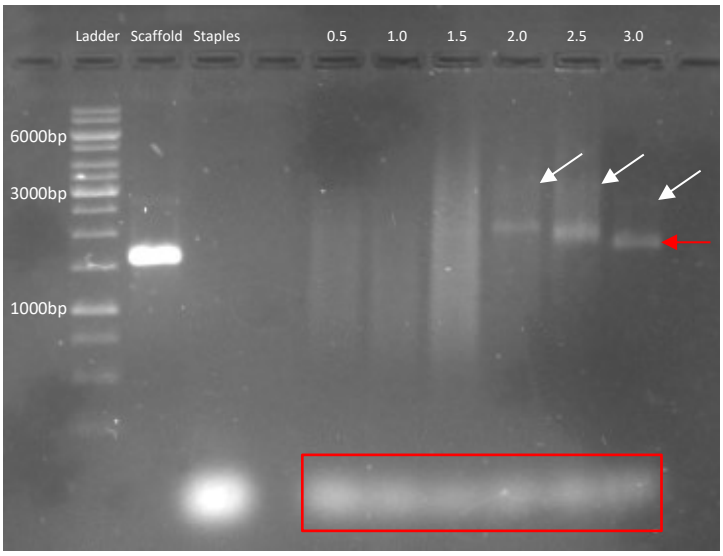

Figure 2-6. AGE image of folding reactions for the second [Mg^{2+}] screen. Lanes numbered 0.5 through 3.0 correspond to folding reactions with increasing [Mg^{2+}] from 0.5 to 3.0mM. Red arrow indicates folded origami at approximately 2,000bp and white arrows indicate faint, slower migrating bands.

Based on the results of this second [Mg^{2+}] screen (Fig. 2-6), it appears that the folding reactions with concentrations of 0.5mM, 1.0mM, and 1.5mM Mg^{2+} did not have much successful folding. Structures of DNA origami in those three lanes are likely only partially folded or could also be misfolded. Folding reactions with Mg^{2+} concentrations

of 2.0mM and 2.5mM showed less smearing below 2,000 bp when compared to the first three lanes, but there was still some smearing observed above the bright bands near 2,000 bp. The best separation appears to have occurred in the lane with 3.0mM Mg^{2+} (red arrow) in the folding reaction mixture. It is interesting to note the presence of a faint band (white arrows) in each of lanes 2.0, 2.5, and 3.0; it is possible that the folded DNA origami could have formed duplexes, or multiplexes. Virtually no smearing is observed in lane 3.0 when compared to the smearing observed in lanes 2.0 and 2.5, which could indicate that misfolding or multimerization is occurring at lower concentrations of magnesium in the folding reaction mixtures. As it appears, AGE results suggest that lower concentrations of magnesium in the reaction mixtures leads to lower folding yield and potentially lower folding quality of DNA origami nanostructures.

Folding of the rectangular DNA origami nanostructures requires complementarity between the scaffold and staple strands. Full complementarity of the scaffold strand used in this work would result in 7,249 base pairs. However, this is not what is observed through AGE characterization. Bands are only observed to migrate similar distances as the 2,000bp and 3,500bp bands of the ladder, and no bands are visible in line with the 6,000bp or 8,000bp bands of the ladder. This large discrepancy between the amount of base pairs in a fully complemented nanostructure and what is observed in the AGE images can be explained by the folded secondary structure of the fabricated DNA origami nanostructures.

As the staple strands begin to interact with the scaffold strand they may bind with small portions of their sequence as a sort of toehold before fully binding with its complement on the scaffold strand through branch migration. As the staples bind larger

portions of their complement, the staple-scaffold interaction is stabilized and the secondary structure of the nanostructure is displaced.[31] Binding of more staples to their complement causes further displacement to a more compact secondary structure. This could be the reason for the migration of the folded DNA origami nanostructures to the 2,000bp distance rather than the 8,000bp distance. While the folded nanostructures could be comprised of approximately 7,250bp, a folded nanostructure with a more compact secondary structure would be able to migrate more easily through the agarose gel than an unfolded nanostructure with a sprawling secondary structure.

Two samples, one folding reaction made with FB(20) and the other made with FB(30) (containing 2.0 and 3.0mM Mg^{2+}, respectively – Table 2-2), were sent for AFM imaging (Fig. 2-7 A and B) to aid in determining an optimal concentration of Mg^{2+} in the folding reaction mixtures for future folding reactions.

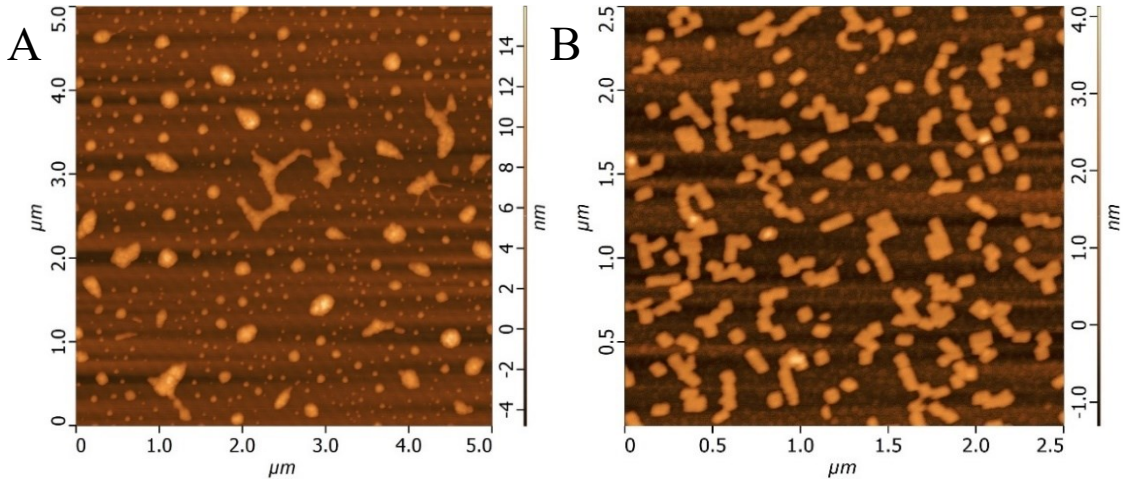

Figure 2-7. AFM images of sample A) R3-2 and B) R3-3, at a 5x5µm scale. [Mg^{2+}] in the folding reaction mixture was (A) 2.0mM and (B) 3.0mM, respectively. AFM imaging performed by Dr. Anatoli Ianoul.

Comparing between Figure 2-7A and 2-7B, the amorphous features observed in the former appear to be similar in size to those observed in latter, but no distinguishable

rectangular DNA origami nanostructures were visible in the former. This could indicate that sample R3-2 (Fig. 2-7A) deposited on the mica surface could have had too high a salt concentration (folding buffer contains sodium and magnesium salts – Chapter 2.3) and may have potentially required further rinsing before imaging. It is also possible that the features present in Figure 2-7A are solely, or primarily, salt features with little to no DNA origami nanostructures present. Divalent cations are required for sample absorption to the mica substrate surface as they mediate the binding of the negatively charged mica surface and phosphate backbone of DNA.[73] Insufficient concentrations of the divalent magnesium ions (Mg^{2+}) in the deposition solution could lead to lower binding of DNA origami nanostructures to the mica substrate and demonstrate no discernible rectangular features, as seen in Fig. 2-7A.

Further analysis of sample R3-3 demonstrates a large number of folded rectangular DNA origami nanostructures (Fig. 2-8A). The right side of the image shows a large amount of closely deposited rectangles with what appears to be significant aggregation of these nanostructures, whereas the left side of the Figure 2-8A shows more dispersed and less aggregated structures. Figure 2-8B is a closer look at the dispersity of these rectangular nanostructures. In this view, the rectangular nanostructures are present in both singular and multi-structure groupings. Singular rectangles are more prevalent on the left side of this image while multi-rectangle groups are more prevalent on the right side of the image.

The difference in dispersity between the left and right side of the AFM images in Figure 2-8 A and B could be caused by aggregation in solution prior to deposition but could also be caused by deposition or sample washing effects. Instead of bridging each

the folded nanostructures to the mica substrate, the magnesium ions in the deposition solution could be bridging the negatively charged phosphate backbones of adjacent rectangular nanostructures. Further rinsing of samples deposited to the mica substrates could potentially mitigate the larger aggregations and lead to more monodispersity in nanostructure imaging but could also wash some nanostructures from the mica substrate surface.

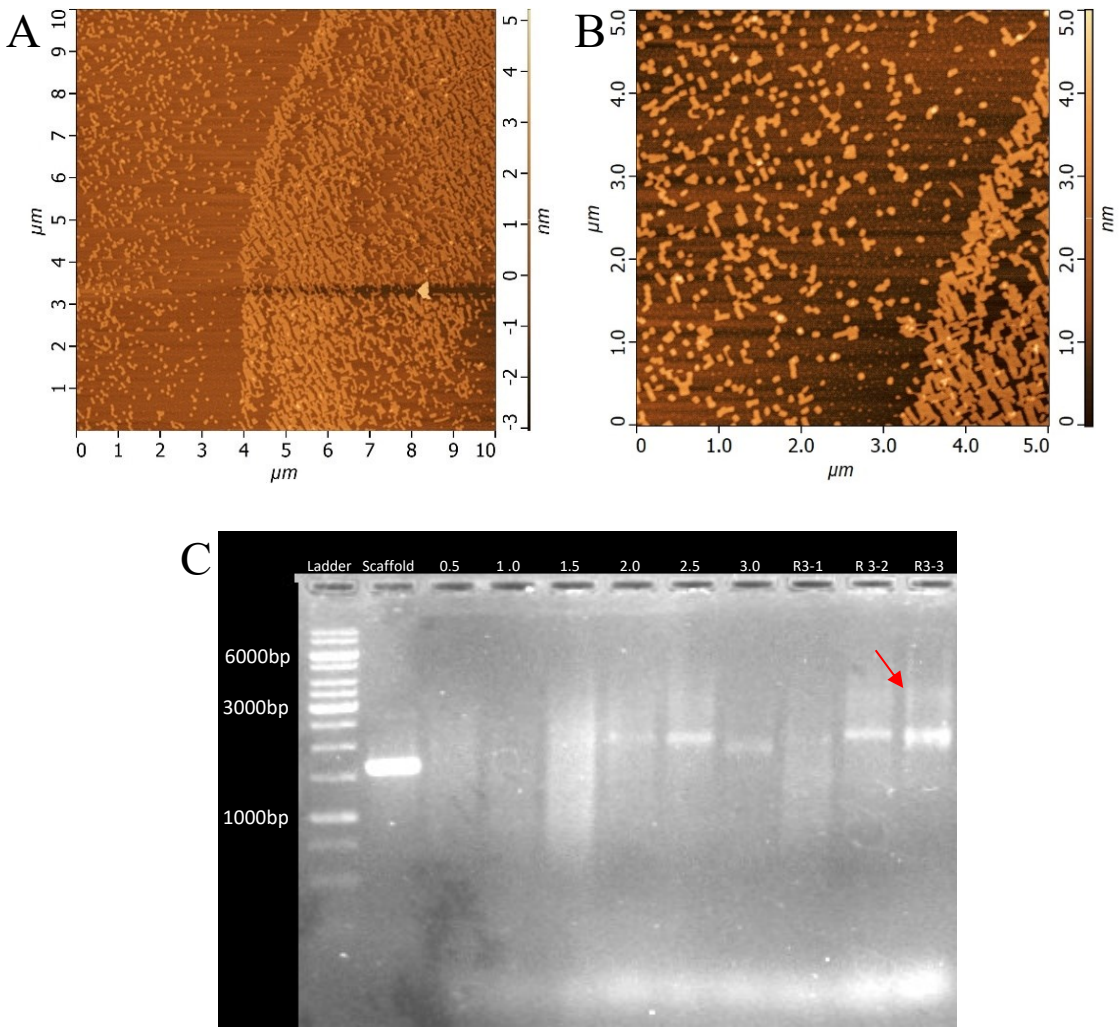

Figure 2-8. AFM image of sample R3-3 at A) a 10x10µm and B) 2.5x2.5 µm scale. [Mg^{2+}] in the folding reaction was 3.0mM. C) AGE image of folding reactions for the [Mg^{2+}] screen and samples sent for AFM imaging. Samples in lanes R3-1, R3-2, and R3-3 were sent for AFM imaging and contained 1.0mM, 2.0mM and 3.0mM Mg^{2+} in the folding reaction mixtures, respectively. AFM imaging performed by Dr. Anatoli Ianoul.

It is apparent from the AGE imaging of a folding reaction using FB(10) (Fig. 2-8C, lane R3-1, [Mg^{2+}] = 1.0mM) that the concentration of magnesium in the folding reaction mixture is inadequate and little properly folded origami is observed, other than a large smearing ranging from approximately 1,000 bp to nearly 3,000 bp. This smearing

effect could be representative of misfolded, or poorly folded DNA origami. Evidence for the use of 2.0mM Mg^{2+} in the folding reaction mixtures was inconclusive. AGE imaging (Fig. 2-8C, lane 3-2) showed a presence of folded structure, but AFM imaging (Fig. 2-7) did not agree. It is known that dsDNA structures, as well as interactions between sticky-ended DNA structures, are stabilized by magnesium ions at physiological levels.[73,81] Concentrations of magnesium ions below, or above, physiological levels tend to destabilize these DNA structures.[73]

The dimensions of DNA origami nanostructures were determined from AFM imaging (Fig. 2-9) as approximately 88 x 63nm with a height between 2-3nm. Single-layered DNA origami nanostructures typically have a height of approximately 2nm, matching the height of the DNA double helix. Height analysis can be challenging as height variances can be caused by differences in sample-tip and substrate-tip interactions.[82]

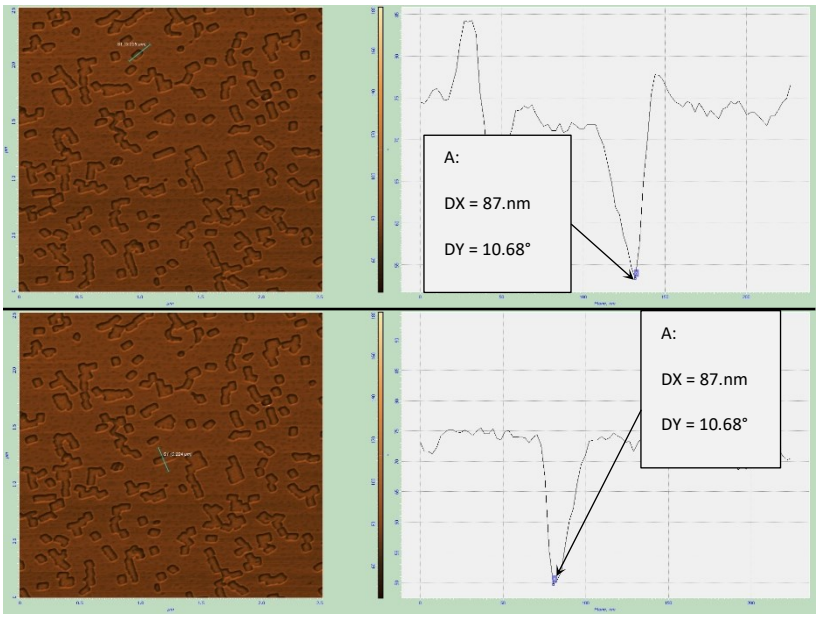

Figure 2-9 Dimensional analysis of AFM images of DNA origami features. Rectangular origami nanostructures were found to have dimensions of approximately 63nm (top) x 88nm (bottom). AFM imaging and analysis performed by Dr. Anatoli Ianoul.

This differs slightly from the dimensions predicted by Tilibit Nanosystems (supplier of scaffold and of staples used for the magnesium screen and AFM imaging) of 94 x 68 x 2.6nm. A reason for this could be differences in imaging techniques such as the use of TEM, or AFM imaging in air compared with imaging in solution. DNA origami could potentially 'shrink', like a sponge losing volume as it dries.

Further folding reactions made use of a folding buffer with a concentration of 3.0mM Mg^{2+} as it appeared to produce the most successful folding of rectangular DNA origami nanostructures. This magnesium concentration in the folding buffer is comparable to *in vivo* magnesium concentrations, allowing for compatibility with *in vivo* applications.

2.4.3 Rothemund rectangle and capture strands

Following confirmation of successful folding of DNA origami nanostructures, a new staple mixture was ordered. The sequences of all staples in the staple mixture ordered from Tilibit Nanosystems were provided, however the location of each of the individual staples was not provided. This staple mixture from Tilibit Nanosystems was based upon the Rothemund rectangular DNA origami[18], but comparing the sequences from the lists of both staple sets did not immediately produce direct similarities.

The purpose for using this new staple mixture was to gain control of the locations for surface modification. Knowledge of the sequences and locations of each staple strand in the DNA origami nanostructure allows for site-specific modifications leading to site-specific target interactions. Select staple strands were modified in order to capture aptamers specifically recognizing thrombin to the surface of the nanostructures.

As previously described, the new staple set was ordered from IDT and was based off Zhao's methods[19], which made use of Rothemund's methods[18], for which the staple sequences and their locations on the DNA origami nanostructure were provided. Capture staple strands (Appendix B: Table 3-3 and Table 3-4) were also ordered from IDT. Folding reactions were performed, as described in Chapter 2.3.1.3, to confirm the folding of DNA origami nanostructures using the new staple mixtures.

Stability of folded DNA origami was briefly observed by AGE. DNA origami folding reaction mixtures were stored at -20°C for one month, after which time some of the stored samples were refolded by subjecting them to the thermal anneal program. The stored folding reaction mixtures and the refolded reaction mixtures were compared with fresh folding reactions following AGE (Fig. 2-10), and the results indicated that folded

DNA origami nanostructures may experience unfolding following periods of storage greater than a month.

Studies have shown that the stability of DNA origami nanostructures can be affected by the length of time that the folded nanostructures, and even staple stock solutions, are stored.[80,83] Staple mixtures, dissolved in diH_2O, can be stored at -20°C for 12 months, but begin to show signs of degradation after 14 months.[80] This is because DNA stored in diH_2O is less stable than DNA stored in Tris-EDTA (TE) and is more susceptible to base damage such as depurination or OH radical-driven oxidative base damage.[83,84] Yields of folded DNA origami decrease as the staple age increases, and folded DNA origami nanostructures also show increased unfolding and degradation.[83]

Table 2-6. Sample nomenclature for the samples fabricated using the Tilibit and Rothemund staple mixtures. The contents of folding reactions listed follow the contents listed in Table 2-3 for the 50µL (A) volume folding reaction, with 20nM concentration of scaffold in the folding reaction mixture.

Sample Description	Sample Notation
Folding Rxn 4 – Tilibit Staple Mixture – Sample 1	R4-1
Folding Rxn 4 – Tilibit Staple Mixture – Sample 1 Refold	R4-11
Folding Rxn 4 – Rothemund Staple Mixture – Sample 5	R4-5
Folding Rxn 4 – Rothemund Staple Mixture – Sample 5 Refold	R4-51
Folding Rxn 5 – Rothemund Capture Mixture – Sample 1	R5-1
Folding Rxn 5 – Rothemund Capture Mixture – Sample 3	R5-3

Experimental results showed that folded DNA origami nanostructures may begin to show signs of unfolding after storage at -20°C for time greater than 1 month. Re-

folding of month-old samples was performed, and the refolded reaction mixtures were compared with the month-old reaction mixtures. It was observed that the month-old nanostructures could be reformed following a re-annealing of the folding reaction mixture (Fig. 2-10, lanes R4-51 and R4-11).

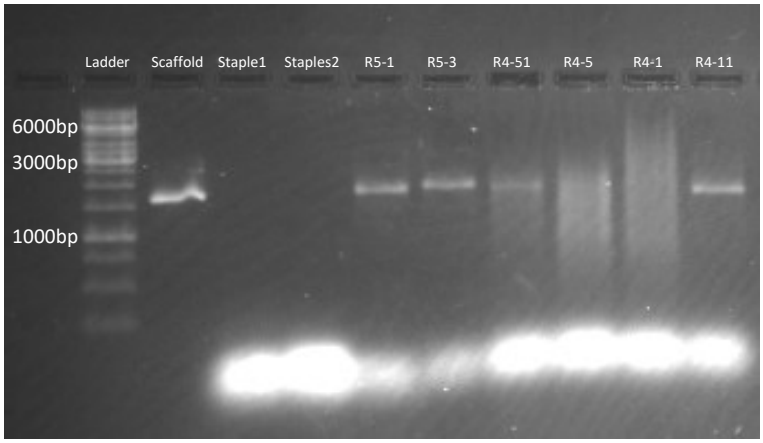

Figure 2-10. AGE image of folded and refolded reaction mixtures. Staple1 indicates the Tilibit staple mixture and Staple2 indicates the Rothemund rectangle staple mixture. Lane R5-1 used the Rothemund rectangle staples (Ch. 2.3.1.2), and lane R5-3 used the Rothemund rectangle staples with the capture staples substituted (Ch. 2.3.1.3). Lanes R4-51 and R4-5 used the Rothemund rectangle staples, while lanes R4-1 and R4-11 used the Tilibit staple mixture.

The folding of DNA origami nanostructures using the Rothemund rectangle staple set, and the capture staple set, can be observed in lanes R5-1 and R5-3 (Fig. 2-10), respectively. Both reaction mixtures produced well-defined bands, indicating well-folded origami nanostructures, and only minute smearing was observed immediately above the bands. Both also produced similar separation when compared with lane 4-11 (from the Tilibit mixture).

Folding reactions R4-1 and R4-5 (lanes R4-1 and R4-5, Fig. 2-10) were stored at 4°C for one month before electrophoresis. Folding reactions R4-11 and R4-51 (lanes R4-

11 and R4-51, Fig. 2-10) were comprised of the same composition as folding reactions R4-1 and R4-5, respectively, and were also stored for one month before being subjected to refolding. These mixtures were refolded by taking the original folding reaction mixture that had been annealed a month prior and subjecting it to the thermal anneal program at the same time as the folding reactions R5-1 and R5-3.

When compared to folding reaction R4-1, sample R4-11 appears to have folded back into properly folded DNA origami nanostructures, while folding reaction R4-1 shows significant unfolding, indicated by the smearing across 500 through 6,000bp. This could indicate a large distribution of partially folded, or partially deteriorated structures. No distinct band appears in lane R4-1, while a distinct band appears in lane R4-11 with minimal smearing present. A similar trend was observed between samples R4-5 and R4-51 which indicates similar unfolding of the month-old folding reaction mixture (Fig. 2-10, lane R4-5) when compared with the refolded reaction mixture (Fig. 2-10, lane R4-51). The difference between the two folding reactions – R4-11 and R4-51 – is that the staple set used with reaction R4-11 was the Tilibit staple mixture, while the staple set used for reaction R4-51 was the Rothemund staple mixture (without capture staple strands).

Fabricated DNA origami nanostructures will exhibit a heterogeneity of folded structures following a folding reaction, regardless of optimized reaction conditions.[67] Folding reaction mixtures are comprised of a large excess of staples with respect to the scaffold, and any staples that are unused for folding the DNA origami may interfere with downstream applications of the nanostructures. In the case of this work, several staple strands were modified to bear extensions that are complementary to extensions on select

aptamers in order to capture the aptamers to the surface of the nanostructures. If there were an excess of capture staple strands free in solution, rather than involved in the formation of the nanostructures, then the result may be reduced yields of aptamers captured to the DNA origami nanostructure's surface. Furthermore, folding reaction mixtures may contain reaction side-products of poorly or misfolded nanostructures in addition to the well-folded nanostructures. Folding reaction mixtures were thus purified by spin-filter centrifugation to remove excess staples and potential folding reaction side-products.

AFM imaging of spin-filter purified Rothemund rectangle with capture staple strands was performed (Fig. 2-11). The size of the features appears to be relatively monodispersed (Fig. 2-11 B and C), but there are several clusters of aggregation present (Fig. 2-11A). The dimensions of the features do not directly match the expected dimensions of the rectangular DNA origami nanostructures that were being fabricated. The Rothemund rectangle is expected to have dimensions or approximately 90x60nm.[18,19] Meanwhile, the dimensions of the nanostructures in Figure 2-11A are observed to be approximately 50x60nm.

It does not seem likely that the features observed in Figure 2-11A are the rectangular DNA origami nanostructures as they do not bear the expected dimensions of the nanostructures. If the nanostructures were indeed produced and may have deposited poorly to the mica substrate surface, then varying height profiles would be expected as the nanostructures would have had to fold over themselves to present significantly smaller dimensions than expected. However, this is not the case as the heights of the features do not far exceed approximately 2nm, which is the expected height of properly

folded single-layer DNA origami nanostructures produced in this work. Thus, these features could potentially be salt residues or artefact on the mica substrate surface following cleavage using clear tape.

It is possible that these features may be poorly folded or incompletely folded DNA origami. But for that to be the case, fragments of varying sizes could be observed for poorly folded structures, and fibrils of the scaffold extending from incompletely folded structures could potentially also be observed.

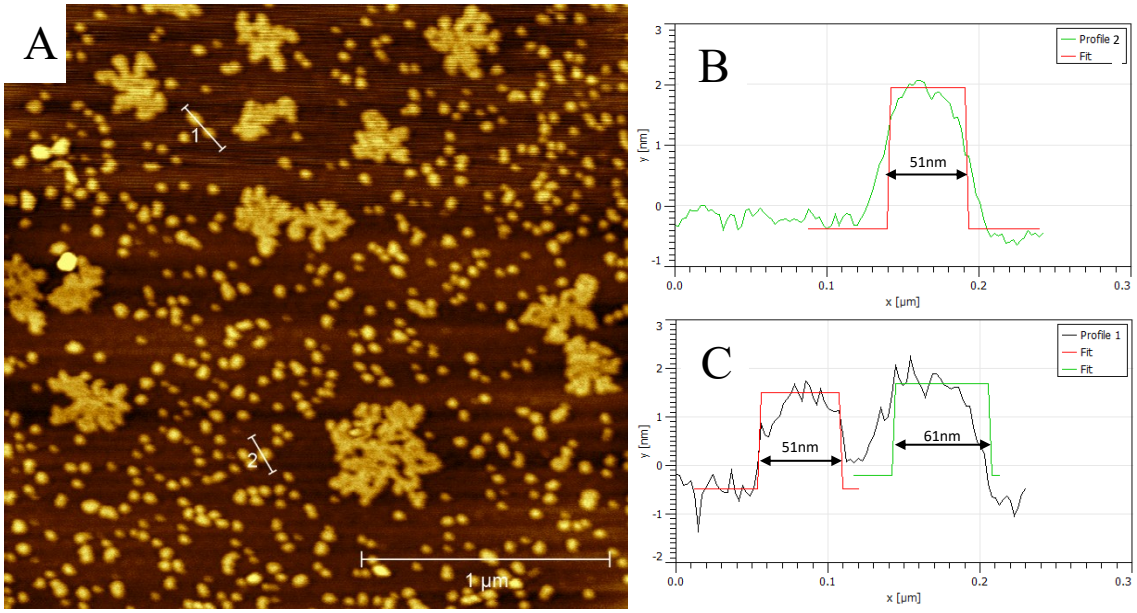

Figure 2-11. A) AFM imaging of DNA origami folding reaction mixture fabricated using Rothemund rectangle with capture staple strands mixture. 1µm scale bar. B) Extracted profile from feature under profile line 2 (A). C) Extracted profiles from feature under profile line 1 (A). AFM imaging performed by Dr. Anatoli Ianoul. Image analysis performed by Fraser Colquhoun.

Analysis of the features observed in Figure 2-11 was inconclusive as to whether the rectangular DNA origami nanostructures had been produced. Another folding reaction mixture was analyzed, and more distinct rectangular nanostructures were observed (Fig. 2-12 A and B), with dimensions similar to the expected dimensions for

these rectangular DNA origami nanostructures. Features were present in the AFM image with dimensions of approximately 82x53nm (Fig. 2-12 C and D), which are more in line with the expected dimensions of 90x60nm than the dimensions of the features observed in Figure 2-11A.

While these features appear to be the rectangular DNA origami nanostructures, not all of the features are rectangular in nature. Some features appear distorted, or larger than the features for which dimensions were determined. In addition, many fragments and fibrils of DNA can be observed in Figure 2-12B (red circles) which appear to hold somewhat rectangular shapes but do not appear to be properly folded nanostructures.

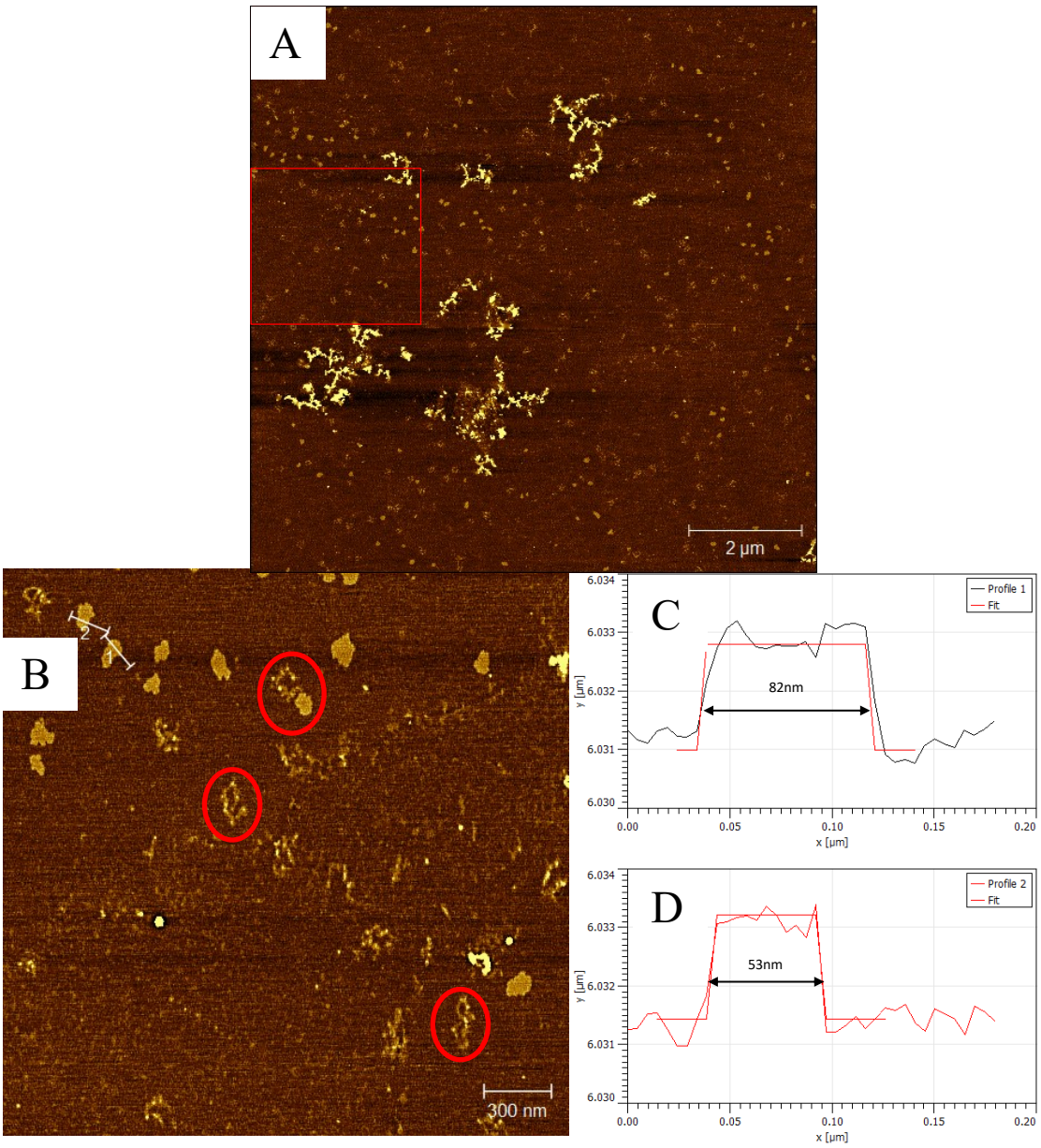

Figure 2-12. AFM images of DNA origami fabricated with Rothemund staple mix with capture strands A) 2µm scale inset. B) magnification of red square from (A) showing some folded DNA origami and many fragments of DNA, 300nm scale inset. C) profile analysis from under line 1 (B) and D) profile analysis from under line 2 (B).

It is unclear at which point the DNA origami nanostructures could have unfolded, but it is likely at a step after the initial folding reaction. Lane R5-3 of Figure 2-10 shows the AGE characterization of the Rothemund rectangle with capture staples and shows no

signs of poor folding, which would be indicated by a smearing effect across a range the gel. Aggregation of folded nanostructures was not readily apparent in this agarose gel image as no distinct bands are observed at higher base pairs (bands in the same lane with less migration through the gel).

The nanostructures observed in Figure 2-12 were purified by spin-filter centrifugation to remove excess staples from the folding reaction mixtures. Unfolding of the nanostructures could have occurred during this step, which could account for many of the fibrils that are observed in Figure 2-12B. The process of centrifugation in the spin filters could also lead to non-specific interactions of the origami nanostructures and possible deformation of the folded structures. The act of deposition from the purified solution to the mica substrate and subsequent rinsing of the substrate surface could also affect the observed shape of the nanostructures. As the DNA origami nanostructures are deposited and the deposition buffer is evaporated or rinsed away, the nanostructures may interact with the mica substrate in a manner that causes them to deform. Imaging samples in solution, rather than in air, may reduce this observed deformation of the rectangular nanostructures.

2.4.4 Aptamer capture

Fabrication of rectangular DNA origami nanostructures using the new staple mixture proved sufficiently promising through AGE and AFM analysis to continue investigating their viability in aptamer-mediated targeted delivery systems. The next step following the fabrication of these nanostructures with capture staple strands incorporated into their structure was to hybridize the aptamers to the capture staple strands.

In this section, folding reactions were purified by centrifugation using spin-filters to remove excess staples and misfolded DNA origami nanostructures. Concentrations of folded structures were calculated by using two different calculations to determine which might provide accurate determinations (Ch. 2.3.2.2). Finally, thrombin-binding aptamers TBA15 and TBA29 were modified with complementary extensions to the capture strands and were incubated with the DNA origami nanostructures to capture the aptamers to their surface.

Rectangular DNA origami nanostructures are fabricated by folding the scaffold strand using staple strands at defined locations. The approximate locations of staple binding are shown in Figure 2-13. Each staple is numbered, and the sequence of each staple is also known. Select staples can be exchanged for modified staples for site-specific addressability. Thrombin-binding aptamers TBA15 and TBA29 were targeted for capture to the surface of the DNA origami nanostructures. Staples 27, 29, 31, 33, and 35 were exchanged for staples with the same sequence but extended with a 15-mer poly-A tail (Fig. 2-13, blue staples). These staples were used for the capture of TBA15 extended with a 15-mer poly-T tail, complementary to the poly-A tail of the capture strands. Similarly, staples 38, 40, 42, 44, and 46 were exchanged for staples with the same sequence but extended with a 15-mer poly-ATA tail (Fig. 2-13, red staples). TBA29 was extended with a 15-mer poly-TAT tail, complementary to the poly-ATA tail of the captures strands. Sequences of the exchanged staples are listed in Table 3-3 and 3-4 of Appendix B.

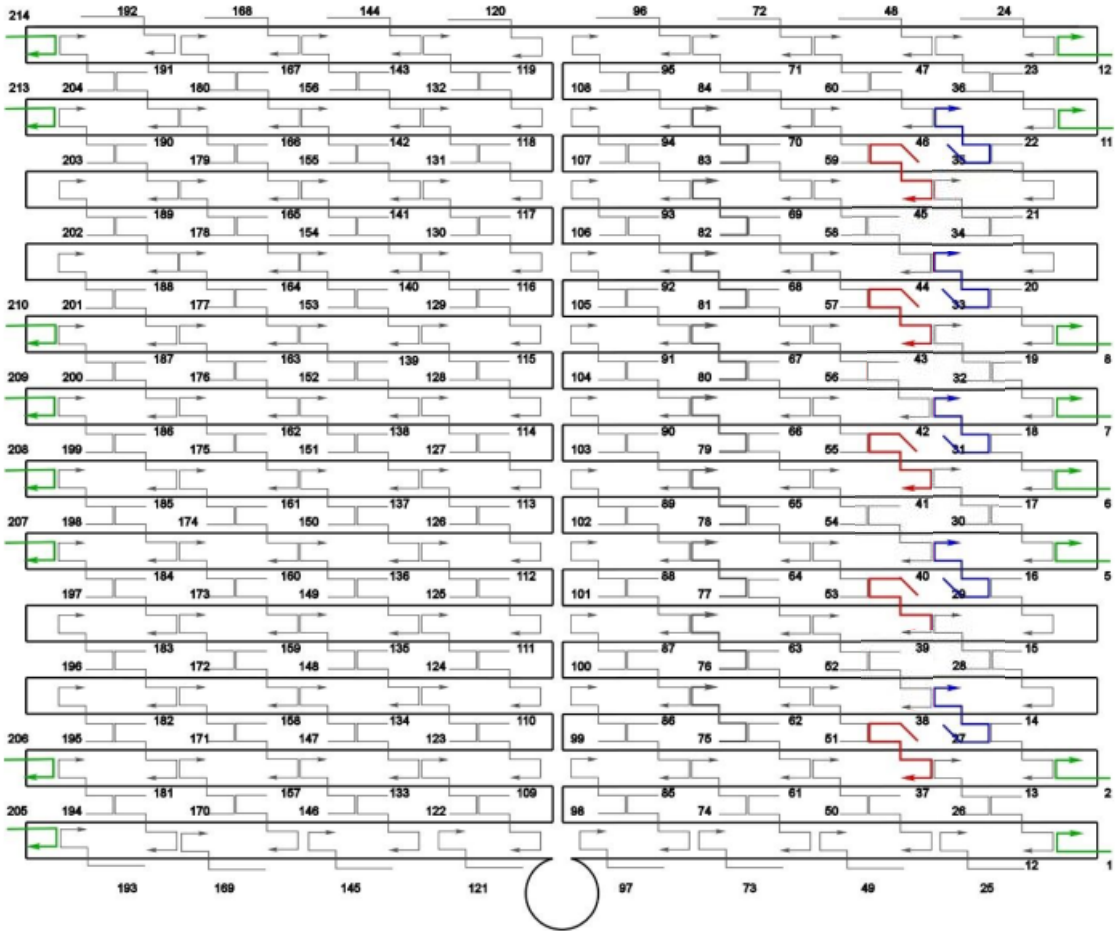

Figure 2-13. Folding of the scaffold strand (black) by staple strands (gray, green, red, and blue). Each staple is numbered to show its location on the surface of the rectangular DNA origami nanostructure. [adapted with permission from Ref.[19]]

The folding reactions producing these DNA origami nanostructures were purified by centrifugation using 100kDa molecular weight cut off (MWCO) spin-filters. Purification by this method was quick and generally produced a 75% recovery of folded structures. Folding reactions may not have had 100% yields and some reaction products may not have been correctly folded and would be filtered out, but the main purpose for purification of folded DNA origami nanostructures is to remove excess staples from the solution so that they do not interfere with further applications of the folded origami.

Loss of product following filtration was theorized to be due to heating within the centrifuge during centrifugation of the reaction mixtures causing denaturation or unfolding of folded nanostructures. However, DNA origami nanostructures have been found to be stable at temperatures of 37°C and only show any signs of unfolding or degradation above 50°C.[20,85] Temperature monitoring, or temperature-controlled centrifugation could provide more evidence related to thermal effects on folded nanostructures.

Some folded products may have been stuck to the spin-filters following centrifugation and may not have been recovered. Spin-filters can be passivated by using proteins or chemicals (e.g. TWEEN, bovine serum albumin, or milk powder) which can reduce non-specific interactions between the DNA origami nanostructures and the column.[69]

Table 2-7. Sample nomenclature for the folding reaction mixtures and aptamer capture reaction mixtures involved in hybridizing aptamers to the surface of DNA origami.

Sample Description	Sample Notation
Folding Rxn 12 – Roth. Capture Mixture – Sample 1	R12-1
Folding Rxn 12 – Roth. Capture Mixture – Sample 2	R12-2
Folding Rxn 12 – Roth. Capture Mixture – Sample 2 Filter-purified	R12-2F
Folding Rxn 12 – Roth. Capture Mixture – Sample 3 Aptamer-conjugated and filter-purified	R12-3A

The concentration of folded DNA origami, as determined by UV-Vis, was approximately 33.6nM (Equation 1). Aptamers TBA15 and TBA29 were annealed with purified DNA origami nanostructures from 45°C to 25°C for five cycles, at a ratio of 3:1 of aptamers to binding sites on DNA origami.

Equation 1 is likely a more accurate determine of the concentration of folded DNA origami nanostructures than Equation 2 as it takes into account the absorbances from each of the components of the folding reaction mixtures. However, the determination of concentration using Equation 1 requires that the absorbances of the staple mixture and the unfiltered folding reaction be measured in addition to the absorbance of the purified folding reaction. Equation 2 is a similar calculation as both Equations 1 and 2 are meant to convert absorbances from ssDNA (i.e., staples and scaffold) to dsDNA (i.e., folded structures). Equation 2 takes the general approximation that the concentration of dsDNA at 1 OD_{260} is 50 mg/mL, and that for ssDNA is 33 mg/mL. Due to the hypochromicity of DNA, extinction coefficients for dsDNA will be less than the sum of the extinction coefficients of the ssDNA of which it is comprised.[86] A lowering of absorbance is observed, which is caused by dipole-induced dipole interactions caused by base stacking.[86,87]

Since the extinction coefficient of the scaffold was given in terms of ssDNA (from IDT OligoAnalyzer) a ratio between the aforementioned concentrations would return an approximation of the concentration of DNA origami at 1 OD_{260}. This assumes that the entire scaffold has become double-stranded with the hybridization of all of the staple strands but will take into account that some of the strands of DNA involved in the fabrication of the DNA origami nanostructures will be ssDNA (e.g., passivation staples at

the nanostructure edges). Analysis of folding reactions demonstrated that purified DNA origami nanostructures were typically produced at a concentration of approximately 30nM.

Purification using spin filters appears to have removed 100% of the excess staples in the folding reactions mixtures. Comparing lanes R12-2F (spin-filter purified) and R12-2 (unpurified) from Figure 2-14 demonstrates the lack of the staples band at the bottom of the image, below the 250 bp ladder band.

Solely examining Figure 2-14, it is difficult to determine with certainty whether the aptamers had been captured to the capture strands on the surface of the DNA origami. Migration of bands in the agarose gel does not differ sufficiently to suggest that there is an increase in base pairing caused by the capture of aptamers to the surface of the nanostructures. Regardless, if aptamers were hybridized to the capture staple strands on the surface of the DNA origami nanostructures, an increase in only 150bp (15bp per aptamer capture x 10 possible aptamer sites) would be observed. Such an increase in base pairing may not be distinguishable at this strength of agarose gel and may not be discernible when comparing to the 1kb ladder reference as the difference between bands in the ladder lane is 500bp. This is supported by comparing the migration of bands between lanes R12-2F and R12-3A (Fig. 2-14) as the migration of the spin-filter purified DNA origami (R12-2F) and the aptamer-conjugated DNA origami (R12-3A) bands do not differ significantly. In order to determine whether the aptamers had been captured to the surface of the DNA origami and to determine the extent of aptamer capture, aptamers could be modified with labels such as Cy5 or Alexa488 and their migration in an agarose gel could be observed and quantified.[19]

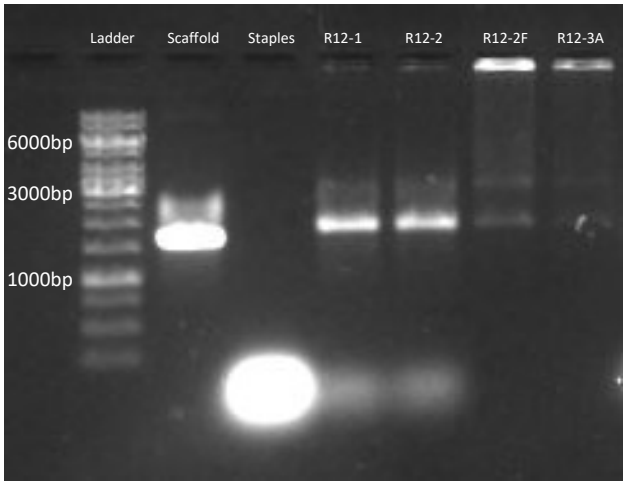

Figure 2-14. AGE image of folding reactions comparing unpurified and purified reaction mixtures. Lanes R12-1 and R12-2 were not purified, while lane R12-2F was purified by spin-filter centrifugation (100kDa MWCO). Lane R12-3A: aptamers were incubated with the purified origami and spin-filter purified (100kDa MWCO) to remove excess aptamers.

The scaffold lane of Figure 2-14 demonstrated similar smearing of its band to that which was observed in previous AGE images of folding reaction mixtures (Fig. 2-10, lane R4-1). This was the first occurrence of this phenomenon in the experiments for this work. The scaffold stock solution had been ordered approximately one year prior to the time that the folding reactions characterized in Figure 2-14 were performed. The scaffold strands in the stock solution may have begun to interact and bind with each other to create larger structures which may have migrated more slowly through the agarose gels than the bright scaffold band. This could potentially be remedied by heating the scaffold stock solution to a denaturing temperature (e.g., >90°C) for a period of time to ensure the scaffold was in its single-stranded form.

Aggregation of the DNA origami nanostructures is observed in lanes R12-2F and R12-3A (Fig. 2-14). Bright bands are observed at the sample wells, indicating that there is significant amount of sample remaining in the wells. Aggregations of the DNA origami

nanostructures may be too large to migrate out of the sample wells and through the agarose gel. Rectangular DNA origami nanostructures have been reported to form chains that are numerous nanostructures in length through what is theorized to be caused by base pairing between passivation tails present on the edges of the DNA origami (Fig. 2-15).[85]

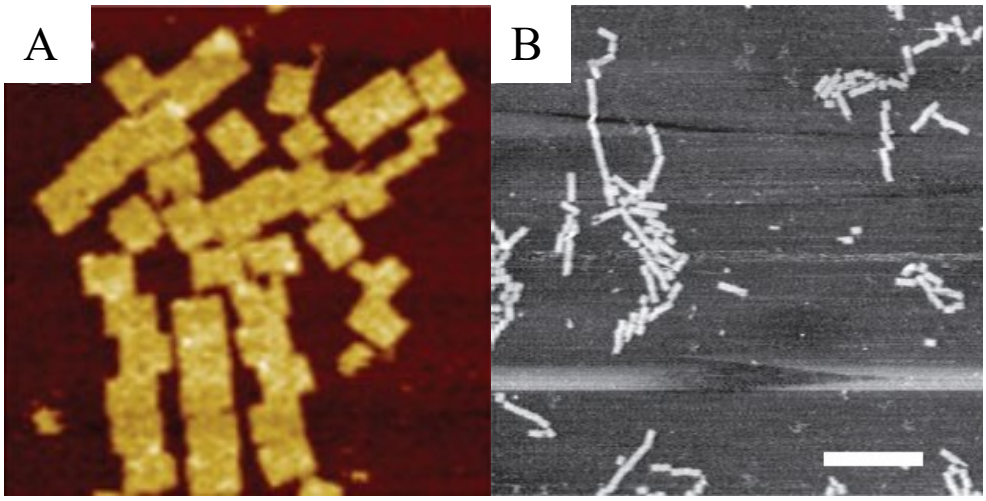

Figure 2-15. A) and B) Rectangular DNA origami nanostructures forming chains and aggregations. [adapted with permission from ref.[31,85]]

Passivation tails are short, poly-T extensions (4 or 5 nucleotides) added to the 5' end of some edge staples in order to limit hybridization or non-specific interactions with other DNA origami nanostructures. While the purpose of the passivation tails of edge staples is to limit interactions between individual nanostructures, the poly-T tails between edge staples of separate nanostructures could potentially interact to create a poly-T bridge between two nanostructures, leading to the formation of chains of DNA origami nanostructures.

Alternatively, the observed aggregation and lack of migration from the sample wells of purified samples, observed in Figure 2-14, could be affected by the concentration of magnesium in the sample solution. Higher concentrations of Mg^{2+} (0.5-5.0mM) have

been shown to cause severe aggregation of nanostructures, with bands disappearing from the agarose gels as the samples remain in the sample wells. This was supported by AFM imaging which demonstrated mostly disordered aggregates of DNA origami nanostructures. The aggregation of nanostructures could possibly be attributed to higher salt concentrations caused by a lyophilization process.[81] Higher salt concentrations could facilitate mismatched base pairs and non-specific interactions.[88] Following the purification of DNA origami nanostructures in this work, the concentrate that was collected may have been too concentrated or the salt concentration from the folding buffer and Mg^{2+} ions may have been too high, resulting in non-specific interactions and aggregation of multiple nanostructures.

Aptamer-conjugated DNA origami nanostructures were imaged by AFM (Fig. 2-16) and large quantities of folded nanostructures were visible. Not all of the features visible in Figure 2-16 A and B are well-defined rectangular nanostructures as was expected, but there is a significant number of folded nanostructures present in the images. Of the folded rectangular nanostructures, dimensions were observed at approximately 87x42nm (Fig. 2-16 C and D). Many of the nanostructures that are observed in Figure 2-16B appear to have once been rectangular in shape but seem to have been deformed to varying degrees. These nanostructures appear to have been stretched, compressed, or pulled apart, possibly from mechanical deformation through spin-filter centrifugation, or through deposition and subsequent rinsing prior to AFM imaging.

What is interesting to note is that there is less aggregation present that is similar to what was observed in Figure 2-8 A and B, where rectangular DNA origami nanostructures would interact edge-to-edge or end-to-end and produce large plates

comprised of multiple origami nanostructures. In Figure 2-16B it can be seen that many of the rectangular nanostructures are linked together in chains.

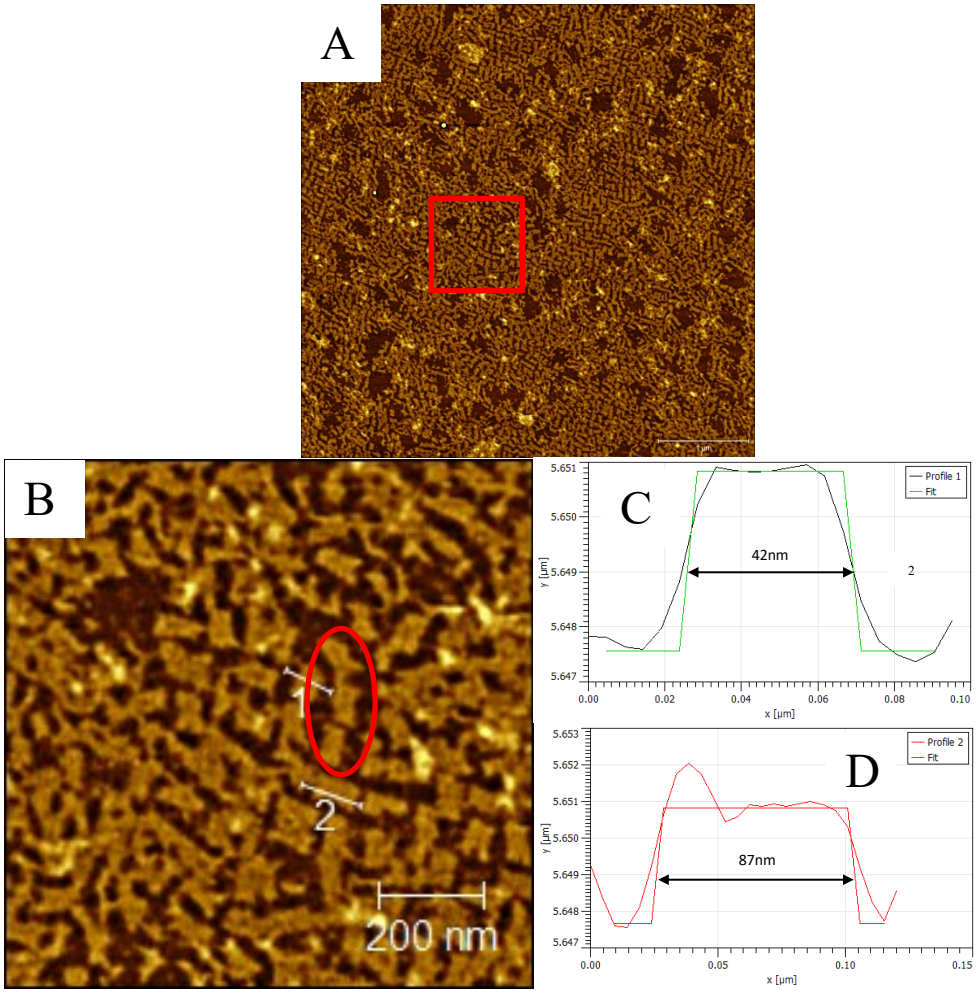

Figure 2-16. AFM imaging of aptamer-conjugated rectangular DNA origami nanostructures. A) large-scale view of aptamer-conjugated origami, 1µm scale inset. B) magnification of the features within the red box from (A), 200nm scale inset. C) profile analysis from under line 1 (B). D) profile analysis from under line 2 (B). AFM imaging performed by Dr. Anatoli Ianoul. Image analysis performed by Fraser Colquhoun.

The linking of these origami nanostructures could be caused by interactions between misfolded, or unfolded nanostructures. For example, a staple which bears a sequence for a portion of one section of the scaffold strand and is programmed for a

crossover to another section of the scaffold strand could hybridize with one portion of the crossover on one scaffold strand, and the other portion of the crossover on another scaffold strand. unfolded or misfolded origami nanostructures could also interact with other nanostructures in non-specific base pairing.

Another possibility for the existence of these DNA origami nanostructure chains is the interaction between capture staple strands and passivation tails on the edges of the nanostructures. As seen under the red oval on Figure 2-16B, three rectangular origami nanostructures are linked together in a short chain through end-to-end interactions. It is possible that the poly-A tails of the capture staple strands of one nanostructure could hybridize with the poly-T passivation tails on the edges of adjacent origami nanostructures creating the observed chain of nanostructures. Future aptamer capture experiments could investigate varying the sequence of capture staple strand extensions from strictly poly-A or poly-T to a combination of A and T in the capture sequence (e.g., AAA TTT AAA TTT AAA), as well as investigating slower annealing programs for aptamer capture.

2.4.5 Thrombin binding

Finally, aptamer-conjugated DNA origami nanostructures were incubated with the target that the aptamers were selected for to demonstrate the target recognition capabilities of this DNA origami system.

Purified rectangular DNA origami nanostructures with aptamers hybridized to capture strands on its surface were incubated with human α-thrombin at 25°C for 30 minutes, at a ratio of 10:1 thrombin to aptamer-origami nanostructures. It was anticipated that the thrombin target would bind to the two aptamers, TBA15 and TBA29, conjugated

to the origami nanostructure surfaces, and present a pattern of thrombin that could be visible by AFM. Based on the locations of the aptamer pairs shown in Figure 2-13, it was expected that binding of thrombin would occur at the five locations that the aptamer pairs were captured to the surface of the nanostructures.

The AFM images of Figure 2-17 show the rectangular DNA origami nanostructures and potentially demonstrate the binding of thrombin molecules to their surfaces. In Figure 2-17A, some single nanostructures are visible, but the majority of nanostructures appear to be aggregated into several clusters. In contrast to the deformed nanostructures aggregated into clusters or chains that were observed in Figure 2-16B the rectangular nanostructures observed in Figure 2-17 A and B are well-formed and a majority of the nanostructures have definite rectangular shapes. The nanostructures are not completely perfect however, there are some sections of the AFM image showing unfolded or deformed DNA origami (Fig. 2-17A, red oval).

Dimensions of the rectangular DNA origami nanostructures indicate that the structures are approximately 77x49nm (Fig. 2-17 B and C). These dimensions are somewhat smaller than the expected dimensions of 90x60nm but could be attributed to potential shrinking of DNA origami when imaged in air, or from instrumental and procedural differences when imaging and analyzing the samples. The image analysis reads the profile under the line drawn across a surface feature and interpolates the shape of that feature. The profile of the AFM feature displayed in Figure 2-17C shows a tailing leading up to and travelling away from the plateau of the feature which is caused by the tip-sample convolution effect. This convolution effect can cause dilation of upward convex features imaged by AFM due to the size and geometry of the tip.[89] This can lead

to inaccurate results if the dimensions of the feature have uncertainty due to the tailing effects observed on either side of the profile plateau.

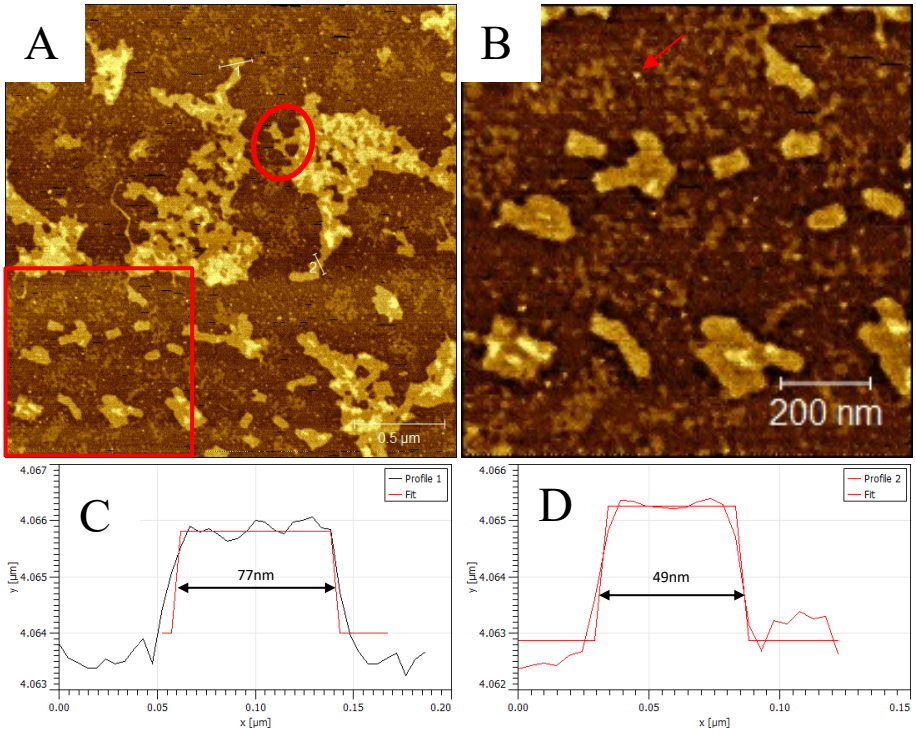

Figure 2-17. AFM images of aptamer-loaded rectangular DNA origami nanostructures following incubation with thrombin. A) Origami nanostructures with several large aggregations, 0.5µm scale inset. Red oval indicating unfolded or deformed nanostructures. B) Magnification of red square from (A), red arrow indicates potential thrombin deposition to the mica substrate. AFM imaging performed by Dr. Anatoli Ianoul. Image analysis performed by Fraser Colquhoun.

Thrombin molecules appear to be present in the AFM images of Figure 2-17 A and B. Small features can be seen between the rectangular origami features (Fig. 2-17A) and are indicated by the red arrow (Fig. 2-17B). As previously described, thrombin molecules were expected to bind to the aptamers which were captured to one end of the rectangular DNA origami nanostructures.

Aptamers captured to the surface of the rectangular DNA origami nanostructures were present in a single row along one edge of the nanostructures (Fig. 2-13, red and blue staples) which would mean that thrombin interacting solely with the thrombin-binding aptamers would be present along the edge of the nanostructures bearing the captured aptamers. The red ovals present on Figure 2-18A indicate locations of possible thrombin binding to the surface of the nanostructures. The marked locations bear a bright spot which could be indicative of thrombin binding to the captured aptamers.

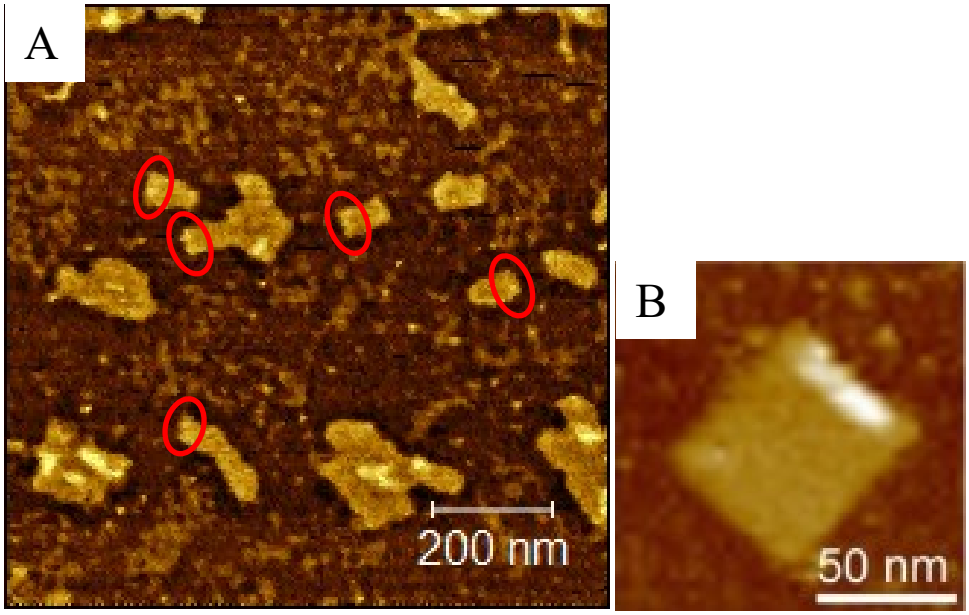

Figure 2-18. A) AFM image of aptamer-loaded rectangular DNA origami nanostructures incubated with thrombin. Red ovals indicate possible thrombin binding to origami nanostructures. AFM imaging performed by Dr. Anatoli Ianoul. Image analysis performed by Fraser Colquhoun. B) AFM image of DNA origami aptarray with bound thrombin (white bar on rectangular DNA origami nanostructure). [adapted with permission from ref.[19]]

Distinct binding of thrombin to the locations of the captured aptamers cannot be definitively concluded from these AFM images. It was expected that thrombin would bind to the five sites on the surface of the nanostructures where pairs of aptamers were

captured, showing five distinct bright spots on each nanostructure surface in the AFM images. The bright spots were expected to be present in a similar manner as the white bar that is observed on the rectangular DNA origami nanostructure in Figure 2-18B. Binding of thrombin to the aptamer-loaded DNA origami nanostructures in this work may have been hindered by ineffective binding to aptamers caused by nanostructure aggregation or ineffective buffer conditions. The fabricated nanostructures could have aggregated through interactions between the capture strands from one nanostructure and the edge passivation tails of a second nanostructure. This could have lead to the overlap of nanostructures and the covering of aptamer capture sites causing the capture sites to be occupied prior to aptamer capture. It is also possible that the buffer (FB) used for the binding of thrombin required more salt components (such as calcium or potassium salts, or phosphates) than were included.

Binding studies of aptamers TBA15 and TBA 29 to thrombin have been carried out in buffers similar to the folding buffer used in this work (50mM Tris-HCl, 100mM NaCl, and 1mM $MgCl_2$ at pH 7.5)[60] as well as with more biologically relevant buffers containing calcium and potassium salts (20mM Tris, 150mM NaCl, 5mM KCl, 1mM $CaCl_2$, and 1mM $MgCl_2$ at pH 7.4)[19,59]. Future experiments making use of a binding buffer containing potassium or calcium salts, or phosphates, could allow for more optimal target binding conditions.[19] In addition, increasing the incubation temperature from 25°C to 37°C, to be more aligned with physiological conditions, could be investigated to determine if there are improvements to the binding of thrombin to the aptamers captured at specific locations on the surface of the DNA origami nanostructures.

2.5 Conclusions

The results presented in this thesis lead to the conclusions that DNA origami nanostructures are a promising technology in their use as an aptamer-mediated targeting system. Rectangular DNA origami nanostructures were fabricated from a DNA origami kit purchased from Tilibit Nanosystems, and were characterized by AGE, UV-Vis spectroscopy, and AFM. A second type of rectangular DNA origami nanostructure was produced from a staple strand mixture with known locations of each staple in the folding route of the scaffold strand. This granted the ability for site-specific modifications of staple strands, allowing for the capture of thrombin-binding aptamers TBA15 and TBA29 to the surface of the nanostructures. Large aggregations and chains of DNA origami nanostructures were observed which could be potentially caused by elevated magnesium concentrations or non-specific interactions following spin-filter centrifugal purification. Thrombin was bound to the nanostructures through recognition by the aptamers captured to the surface of the DNA origami. Binding of targets to captured aptamers demonstrates the ability of DNA origami nanostructures to function as carriers for aptamer-mediated recognition of targets.

Chapter 3: Future Directions

3.1 Folding reactions

Temperature programs in this work made use of annealing rates of 1°C/minute for the self-assembly of DNA origami nanostructures. Slower annealing rates could be employed to investigate differences in the yield of folding reactions with longer annealing times. DNA origami of similar structure were annealed by Zhao[19] at a rate ten times slower than the annealing rate reported here.

An area of interest for all chemists and industry personnel is the scalability of chemical reactions. The majority of DNA origami nanostructure fabrication methods utilize small folding reaction volumes (50-100μL), which may be due to limited allowable tube sizes in thermal cyclers. It has been reported that folding reactions in large volumes of 20mL (as opposed to typical 100μL in methods such as Rothemund's[18]) have produced DNA origami nanostructures with yields in the milligram range. Production of large amounts of DNA origami could aid in investigations of its applications without the time-consuming need to complete folding reactions for each individual trial application.

3.2 Purification and characterization

The extraction of folded DNA origami nanostructures from folding reaction mixtures is important for its downstream uses. Without the removal of excess staple strands or misfolded structures any further use of folded DNA origami could be hampered past the initial folding reaction and characterization.

Purification by centrifugation with spin-filter columns (Amicon) is a quick method for removal of excess staple strands and structures under the molecular weight cut-off. Other purification methods that could be investigated include PEG precipitation, size exclusion columns, fast protein liquid chromatography, and magnetic bead capture.[69]

AGE is also a common method for DNA purification and has been used for the purification of DNA origami. However, AGE extraction typically results in low recoveries and dilute solutions of purified materials.[70]

AGE is frequently used for separation and purification of DNA but was not used for purification in this work. Removal of bands from agarose gels requires manual excision of bands and removal of agarose gel from around the sample band contained within the excised gel. It was thought that the use of typical chaotropic denaturing agents, urea and guanidium chloride (GdmCl), could have negative effects on the structure of folded origami. However, it has been shown that DNA origami nanostructures are stable at room temperature in concentrations of denaturing agents of up to 6M. Structural stability began to decrease at temperatures above 50°C for DNA origami in urea (1-4M urea) and above 37°C in GdmCl (1-4M GdmCl).[90] A freeze and squeeze method can also be used for the extraction of bands from agarose gels.[67]

AGE could be used in the future for purification of folded DNA origami nanostructures if the sample volumes were larger. Although, there are other purification methods, such as PEG precipitation, that can produce significantly better recoveries of folded DNA origami.[69]

PEG precipitation has been previously investigated for DNA origami purification[19,67,69] and has been shown to recover DNA origami nanostructures at a higher percentage when compared with centrifugation in spin-filter columns (>90% vs. >50%)[70] and could be a strong purification method to investigate.

Characterization of DNA origami nanostructures is typically performed by visualization of bands by AGE, imaging folded structures by AFM or TEM, and

quantification of folded products by UV-Vis. Similar to the modification of staples in this study for the capture of thrombin aptamers, staple or aptamer sequences could be modified or functionalized to bear fluorescent labels such as Cy5 or Alexa488.[19] These labels could be viewed following AGE or quantified by UV-Vis to determine the concentration of DNA origami nanostructures, or too determine the extent of aptamer capture (in the case of aptamer labeling).

While UV-Vis is frequently the method used for quantification, AFM has also been employed to determine concentrations of folded DNA origami where folded nanostructures are counted per unit area.[19]

3.3 Future applications of DNA origami

The next step past the confirmation of binding of the target to an aptamer docked on the surface of the DNA origami is to be able to control the release of the target from the aptamer, or of the aptamer-target complex from the surface of the origami. One method that could be employed is the use of 'antidote' strands which are ssDNA strands that are complementary to the sequence of the aptamers used to bind a target. Following the binding of aptamer to its target, it has been shown that the addition of an antidote strand was able to reverse the binding of aptamer and target and release the target back into solution.[19] A downside to this method is that the aptamer is still bound to the surface of the DNA origami nanostructure but is now hybridized to its complement, leaving the surface of the nanostructure inert to binding of future targets.

Another method for target release could come from a pH-controlled switch. It has been reported[91] that under neutral conditions, a thrombin-binding aptamer modified with a poly-A tail at its 3' end folds into its G-quadruplex (Fig. 2-1) conformation and binds

thrombin. Under acidic conditions, the thrombin aptamer forms A-G mispairs that drive the formation of a stem-loop structure causing the release of thrombin.[91] The formation of the stem-loop structure could also lead to the release of the aptamers from the surface of the DNA origami nanostructures. Changes in pH may also affect the stability of folded DNA origami nanostructures, or their ability to bear molecular payloads. This can be advantageous for applications such as the targeted delivery of anti-cancer drugs to tumor cells. Interactions between DNA origami nanostructures and their drug payloads may be affected by the lower pH of the intracellular environments of tumor cells causing a release of the drugs loaded into the nanostructures.[42]

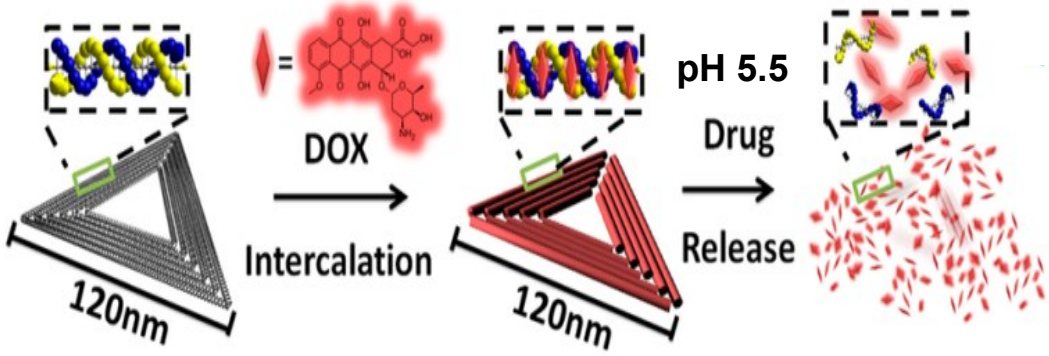

Figure 3-1. Loading of doxorubicin (DOX) into triangular DNA origami nanostructures with subsequent release of intercalated DOX following a change in pH (pH 7.4 to pH 5.5). [adapted with permission from ref.[42]]

Similar to the work that was performed in Zhao's methods, as well as the work in this thesis, DNA origami nanostructures could be used to target thrombin using a pair of thrombin-binding aptamers captured to the surface of the DNA origami. However, instead of using a pair of aptamers captured on the surface of the DNA origami, acting as a set of tweezers, an extended aptamer that bears both TBA15 and TBA29 could be used (Fig. 3-1).

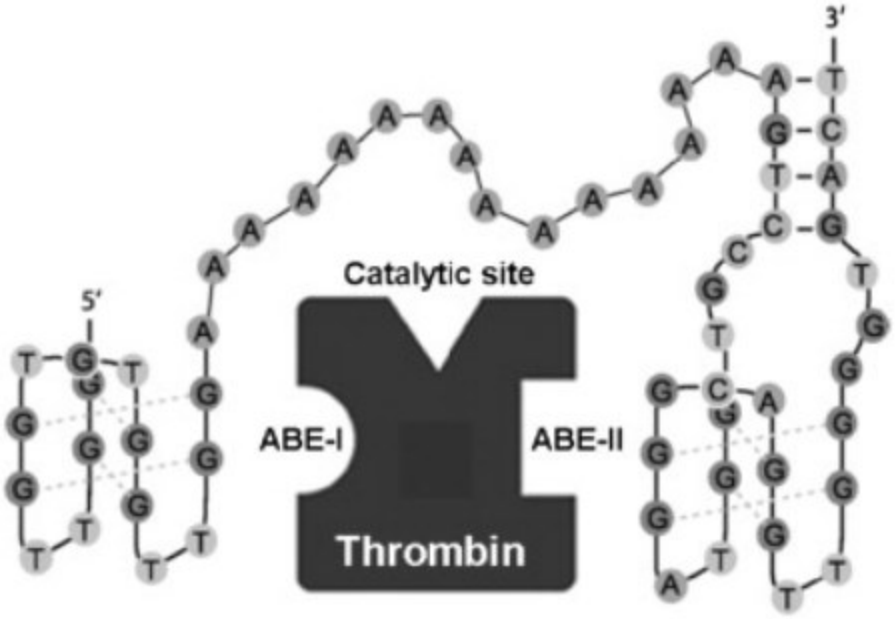

Figure 3-2. Aptamers TBA15 and TBA29 connected by a poly-A linker for the binding of thrombin exosites I and II. [adapted with permission from ref.[61]]

TBA29 has a better K_d when compared with that of TBA15 (~0.5nM vs ~100nM)[59,60] and therefore its end of the aptamer could be free to flagellate while the TBA15 end of the connected aptamer pair was captured to the surface of DNA origami by a poly-A or poly-T tail.

3.4 Conclusions

In conclusion, DNA origami nanostructures show promise for applications in biological and medical fields, including their application in targeted delivery systems. Future work could investigate optimizations of temperature programs and folding reaction buffer conditions to improve the yield of fabricated nanostructures, as well as investigate different purification techniques (e.g., PEG precipitation) to increase the recovery of properly folded DNA origami nanostructures from folding reaction mixtures. In addition, future studies of DNA origami nanostructures could investigate the capture

and controlled release of targets by altering the pH of the nanostructure environment. Finally, aptamer-mediated recognition and binding of thrombin to DNA origami nanostructures could be improved by employing the TBA15 and TBA29 combination aptamer (Fig. 3-2), and by altering the composition of aptamer capture sequences so that they may only hybridize to their complementary extension on the desired aptamers and not have any interaction with other nanostructures that could cause chains or aggregations to form.

Appendices

Appendix A

A.1 Extraction of bands following AGE

Freeze and Squeeze

A method for the extraction of purified DNA origami nanostructures from bands in agarose gels was performed in this work, with mild results. Samples were electrophoresed, as described in Chapter 2.3.1.4, and bands were viewed by UV illumination using the AlphaImager.

Selected bands were excised using a razor blade and excess agarose was trimmed. The excised bands were transferred to a spin-filter column (30kDa MWCO) in a 2mL tube, and the tube was placed in a -20°C freezer for 5-10 minutes. The sample was centrifuged at 12,000 x g for 5 minutes and the volume of flowthrough was measured by pipetting. Extracted samples were electrophoresed again on the following AGE trial (Fig. 3-1).

It is apparent that no significant amount of sample was visible in any of the three lanes of extracted material (Fig. A-1, lanes E-Sc, E-St, E-2-4). There is a faint band appearing in the extracted scaffold and staple lanes, but not an amount that would suggest sufficient recovery had occurred. It is obvious that further optimization of this method is required if AGE is to be used as a purification method for purifying DNA origami nanostructures.

Possible improvements include the use of higher molecular weight cut off filters (100kDa used for DNA origami), flash freezing the excised bands in liquid nitrogen, and

ethanol precipitation to form a pellet that can be resuspended in a known volume of solvent.

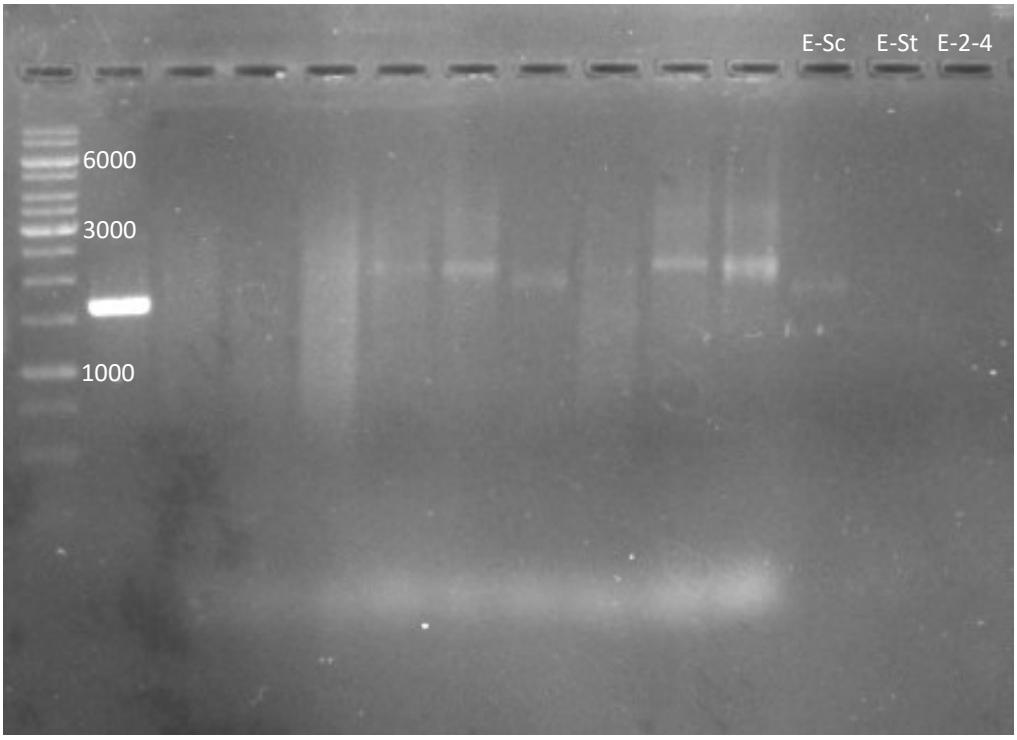

Figure A-1. AGE image of bands extracted from previous AGE trial. Bands containing scaffold, staples, and reaction mixtures were excised from a gel and extraction from the agarose gel by Freeze and Squeeze method. E-Sc is the extracted scaffold lane, E-St is the extracted staple lane, and E-2-4 is the extracted band of folding reaction 2-4.

A.2 Other issues with AGE

One of the aspects of AGE that were investigated in early trials was the effect of soaking the agarose gel in SYBR after the gel had been electrophoresed, rather than adding SYBR to the molten agarose before it is cast. Product details (Thermo Fisher Scientific) described methods where the staining of the gel by SYBR may be performed before the gel is cast, or after the gel is cast.

The agarose gel was soaked in 200mL of 0.5xTBE with 20µL of SYBR for 30 minutes, protected from light. Figure A-2 shows the image of the gel following post-electrophoresis soaking. It can be seen that the distinction between higher bp bands in the ladder lanes is much worse than for bands viewed in images following AGE with the addition of SYBR to molten agarose.

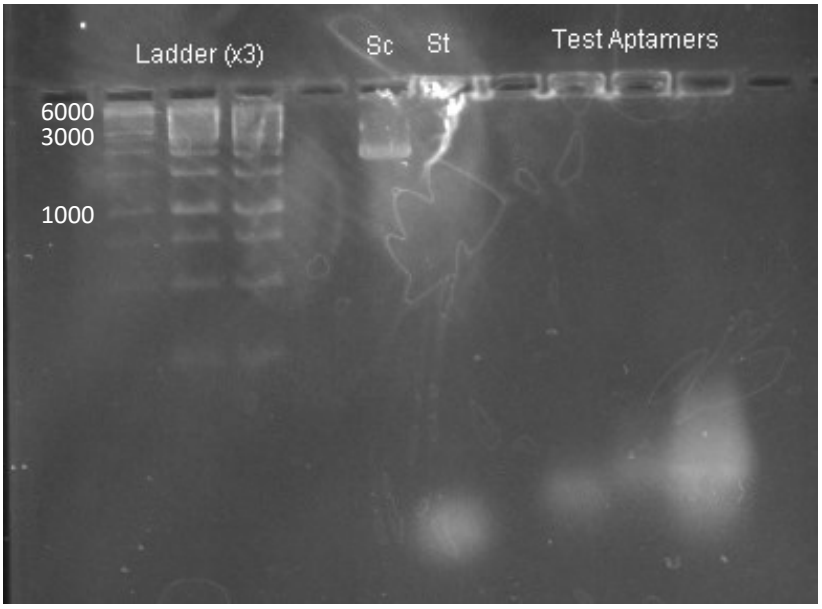

Figure A-2. Agarose gel of test aptamers stained with SYBR after electrophoresis. The gel was removed from its cast and soaked in 200mL of 0.5xTBE with 20µL SYBR for 30 minutes, protected from light.

Another component in the preparation of AGE that was optimized was the temperature at which the agarose gel was poured into the gel cast tray. The agarose powder is dissolved by combining with 0.5xTBE and heating in a microwave until all agarose had dissolved. The molten agarose solution was left to cool at room temperature to an acceptable temperature so that it did not damage the acrylic gel cast tray when poured. Optimal temperatures for pouring the agarose gel into the cast were between 55

and 60°C. Pouring at temperatures higher than 60°C could lead to damage of the acrylic tray and pouring at temperatures lower than 50°C led to poorly formed wells.

Molten agarose gel temperatures were measured using a thermometer that was only inserted into the agarose solution until a stable temperature was observed. Between temperature readings, the temperature of the agarose gel had fallen sufficiently that when the gel was poured it did not spread evenly throughout the casting tray and the wells were not formed properly (Fig. A-3).

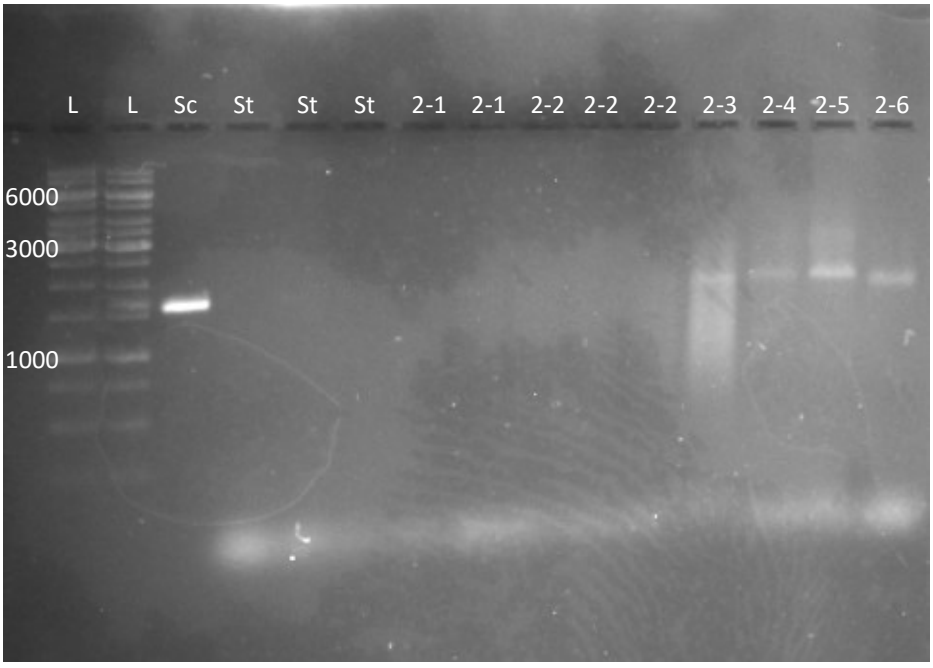

Figure A-3. Issue with well formation, gel was poured at around 50°C and wells did not form properly, leading to sample spillover into adjacent wells. The agarose gel should have been poured when the temperature of the gel between 55 and 60°C.

Samples were added to the wells and many of these samples simply poured over the edge of the well into which they were pipetted and began filling adjacent wells. As can be seen in Figure A-3, there are two lanes bearing the 1 kb ladder, three lanes containing the staple mixture, and multiple lanes visible for samples 2-1 and 2-2.

Following this AGE experiment, all agarose gels were monitored more closely and were poured when the temperature of the molten agarose was between 55 – 60°C.

As each AGE trial proceeded, the running buffer would heat up and eventually show a precipitation over the negative electrode within the buffer solution. Precipitation of salts from the running buffer could be disadvantageous for separation of bands within the agarose gels as there would be a loss of ions in solution and therefor a loss of mobility of the DNA being separated in the gel. In future experiments, a cooling basin could be employed to bath the gel cast system in cool water to dissipate heating of the buffer ad reduce precipitation of salts. Another possibility is the attachment of a buffer exchanger which would recirculate buffer and also allow for dissipation of heat and minimal precipitation of salts from the buffer.

Appendix B

B.1 Staple sequences used for Rothemund rectangles and capture strands

Table 3-1. Sequences of unmodified staple strands of rectangular DNA origami.

Staple	Sequence (5' – 3')
S13	TGG TTT TTA ACG TCA AAG GGC GAA GAA CCA TC
S14	CTT GCA TGC ATT AAT GAA TCG GCC CGC CAG GG
S15	TAG ATG GGG GGT AAC GCC AGG GTT GTG CCA AG
S16	CAT GTC AAG ATT CTC CGT GGG AAC CGT TGG TG
S17	CTG TAA TAT TGC CTG AGA GTC TGG AAA ACT AG
S18	TGC AAC TAA GCA ATA AAG CCT CAG TTA TGA CC
S19	AAA CAG TTG ATG GCT TAG AGC TTA TTT AAA TA
S20	ACG AAC TAG CGT CCA ATA CTG CGG AAT GCT TT
S21	CTT TGA AAA GAA CTG GCT CAT TAT TTA ATA AA
S22	ACG GCT ACT TAC TTA GCC GGA ACG CTG ACC AA
S23	GAG AAT AGC TTT TGC GGG ATC GTC GGG TAG CA
S24	ACG TTA GTA AAT GAA TTT TCT GTA AGC GGA GT
S25	ACC CAA ATC AAG TTT TTT GGG GTC AAA GAA CG
S26	TGG ACT CCC TTT TCA CCA GTG AGA CCT GTC GT
S27	GCC AGC TGC CTG CAG GTC GAC TCT GCA AGG CG
S28	ATT AAG TTC GCA TCG TAA CCG TGC GAG TAA CA
S29	ACC CGT CGT CAT ATG TAC CCC GGT AAA GGC TA

S30	TCA GGT CAC TTT TGC GGG AGA AGC AGA ATT AG
S31	CAA AAT TAA AGT ACG GTG TCT GGA AGA GGT CA
S32	TTT TTG CGC AGA AAA CGA GAA TGA ATG TTT AG
S33	ACT GGA TAA CGG AAC AAC ATT ATT ACC TTA TG
S34	CGA TTT TAG AGG ACA GAT GAA CGG CGC GAC CT
S35	GCT CCA TGA GAG GCT TTG AGG ACT AGG GAG TT
S36	AAA GGC CGA AAG GAA CAA CTA AAG CTT TCC AG
S37	AGC TGA TTA CAA GAG TCC ACT ATT GAG GTG CC
S38	CCC GGG TAC TTT CCA GTC GGG AAA CGG GCA AC
S39	GTT TGA GGG AAA GGG GGA TGT GCT AGA GGA TC
S40	AGA AAA GCA ACA TTA AAT GTG AGC ATC TGC CA
S41	CAA CGC AAT TTT TGA GAG ATC TAC TGA TAA TC
S42	TCC ATA TAC ATA CAG GCA AGG CAA CTT TAT TT
S43	CAA AAA TCA TTG CTC CTT TTG ATA AGT TTC AT
S44	AAA GAT TCA GGG GGT AAT AGT AAA CCA TAA AT
S45	CCA GGC GCT TAA TCA TTG TGA ATT ACA GGT AG
S46	TTT CAT GAA AAT TGT GTC GAA ATC TGT ACA GA
S47	AAT AAT AAG GTC GCT GAG GCT TGC AAA GAC TT
S48	CGT AAC GAT CTA AAG TTT TGT CGT GAA TTG CG
S49	GTA AAG CAC TAA ATC GGA ACC CTA GTT GTT CC
S50	AGT TTG GAG CCC TTC ACC GCC TGG TTG CGC TC
S51	ACT GCC CGC CGA GCT CGA ATT CGT TAT TAC GC
S52	CAG CTG GCG GAC GAC GAC AGT ATC GTA GCC AG

S53	CTT TCA TCC CCA AAA ACA GGA AGA CCG GAG AG
S54	GGT AGC TAG GAT AAA AAT TTT TAG TTA ACA TC
S55	CAA TAA ATA CAG TTG ATT CCC AAT TTA GAG AG
S56	TAC CTT TAA GGT CTT TAC CCT GAC AAA GAA GT
S57	TTT GCC AGA TCA GTT GAG ATT TAG TGG TTT AA
S58	TTT CAA CTA TAG GCT GGC TGA CCT TGT ATC AT
S59	CGC CTG ATG GAA GTT TCC ATT AAA CAT AAC CG
S60	ATA TAT TCT TTT TTC ACG TTG AAA ATA GTT AG
S61	GAG TTG CAC GAG ATA GGG TTG AGT AAG GGA GC
S62	TCA TAG CTA CTC ACA TTA ATT GCG CCC TGA GA
S63	GAA GAT CGG TGC GGG CCT CTT CGC AAT CAT GG
S64	GCA AAT ATC GCG TCT GGC CTT CCT GGC CTC AG
S65	TAT ATT TTA GCT GAT AAA TTA ATG TTG TAT AA
S66	CGA GTA GAA CTA ATA GTA GTA GCA AAC CCT CA
S67	TCA GAA GCC TCC AAC AGG TCA GGA TCT GCG AA
S68	CAT TCA ACG CGA GAG GCT TTT GCA TAT TAT AG
S69	AGT AAT CTT AAA TTG GGC TTG AGA GAA TAC CA
S70	ATA CGT AAA AGT ACA ACG GAG ATT TCA TCA AG
S71	AAA AAA GGA CAA CCA TCG CCC ACG CGG GTA AA
S72	TGT AGC ATT CCA CAG ACA GCC CTC ATC TCC AA
S73	CCC CGA TTT AGA GCT TGA CGG GGA AAT CAA AA
S74	GAA TAG CCG CAA GCG GTC CAC GCT CCT AAT GA
S75	GTG AGC TAG TTT CCT GTG TGA AAT TTG GGA AG

S76	GGC GAT CGC ACT CCA GCC AGC TTT GCC ATC AA
S77	AAA TAA TTT TAA ATT GTA AAC GTT GAT ATT CA
S78	ACC GTT CTA AAT GCA ATG CCT GAG AGG TGG CA
S79	TCA ATT CTT TTA GTT TGA CCA TTA CCA GAC CG
S80	GAA GCA AAA AAG CGG ATT GCA TCA GAT AAA AA
S81	CCA AAA TAT AAT GCA GAT ACA TAA ACA CCA GA
S82	ACG AGT AGT GAC AAG AAC CGG ATA TAC CAA GC
S83	GCG AAA CAT GCC ACT ACG AAG GCA TGC GCC GA
S84	CAA TGA CAC TCC AAA AGG AGC CTT ACA ACG CC
S85	CCA GCA GGG GCA AAA TCC CTT ATA AAG CCG GC
S86	GCT CAC AAT GTA AAG CCT GGG GTG GGT TTG CC
S87	GCT TCT GGT CAG GCT GCG CAA CTG TGT TAT CC
S88	GTT AAA ATT TTA ACC AAT AGG AAC CCG GCA CC
S89	AGG TAA AGA AAT CAC CAT CAA TAT AAT ATT TT
S90	TCG CAA ATG GGG CGC GAG CTG AAA TAA TGT GT
S91	AAG AGG AAC GAG CTT CAA AGC GAA GAT ACA TT
S92	GGA ATT ACT CGT TTA CCA GAC GAC AAA AGA TT
S93	CCA AAT CAC TTG CCC TGA CGA GAA CGC CAA AA
S94	AAA CGA AAT GAC CCC CAG CGA TTA TTC ATT AC
S95	TCG GTT TAG CTT GAT ACC GAT AGT CCA ACC TA
S96	TGA GTT TCG TCA CCA GTA CAA ACT TAA TTG TA
S97	GAA CGT GGC GAG AAA GGA AGG GAA CAA ACT AT
S98	CCG AAA TCC GAA AAT CCT GTT TGA AGC CGG AA

S99	GCA TAA AGT TCC ACA CAA CAT ACG AAG CGC CA
S100	TTC GCC ATT GCC GGA AAC CAG GCA TTA AAT CA
S101	GCT CAT TTT CGC ATT AAA TTT TTG AGC TTA GA
S102	AGA CAG TCA TTC AAA AGG GTG AGA AGC TAT AT
S103	TTT CAT TTG GTC AAT AAC CTG TTT ATA TCG CG
S104	TTT TAA TTG CCC GAA AGA CTT CAA AAC ACT AT
S105	CAT AAC CCG AGG CAT AGT AAG AGC TTT TTA AG
S106	GAA TAA GGA CGT AAC AAA GCT GCT CTA AAA CA
S107	CTC ATC TTG AGG CAA AAG AAT ACA GTG AAT TT
S108	CTT AAA CAT CAG CTT GCT TTC GAG CGT AAC AC
S109	ACG AAC CAA AAC ATC GCC ATT AAA TGG TGG TT
S110	CGA CAA CTA AGT ATT AGA CTT TAC AAT ACC GA
S111	CTT TTA CAC AGA TGA ATA TAC AGT AAA CAA TT
S112	TTA AGA CGT TGA AAA CAT AGC GAT AAC AGT AC
S113	GCG TTA TAG AAA AAG CCT GTT TAG AAG GCC GG
S114	ATC GGC TGC GAG CAT GTA GAA ACC TAT CAT AT
S115	CCT AAT TTA CGC TAA CGA GCG TCT AAT CAA TA
S116	AAA AGT AAT ATC TTA CCG AAG CCC TTC CAG AG
S117	TTA TTC ATA GGG AAG GTA AAT ATT CAT TCA GT
S118	GAG CCG CCC CAC CAC CGG AAC CGC GAC GGA AA
S119	AAT GCC CCG TAA CAG TGC CCG TAT CTC CCT CA
S120	CAA GCC CAA TAG GAA CCC ATG TAC AAA CAG TT
S121	CGG CCT TGC TGG TAA TAT CCA GAA CGA ACT GA

S122	TAG CCC TAC CAG CAG AAG ATA AAA ACA TTT GA
S123	GGA TTT AGC GTA TTA AAT CCT TTG TTT TCA GG
S124	TTT AAC GTT CGG GAG AAA CAA TAA TTT TCC CT
S125	TAG AAT CCC TGA GAA GAG TCA ATA GGA ATC AT
S126	AAT TAC TAC AAA TTC TTA CCA GTA ATC CCA TC
S127	CTA ATT TAT CTT TCC TTA TCA TTC ATC CTG AA
S128	TCT TAC CAG CCA GTT ACA AAA TAA ATG AAA TA
S129	GCA ATA GCG CAG ATA GCC GAA CAA TTC AAC CG
S130	ATT GAG GGT AAA GGT GAA TTA TCA ATC ACC GG
S131	AAC CAG AGA CCC TCA GAA CCG CCA GGG GTC AG
S132	TGC CTT GAC TGC CTA TTT CGG AAC AGG GAT AG
S133	AGG CGG TCA TTA GTC TTT AAT GCG CAA TAT TA
S134	TTA TTA ATG CCG TCA ATA GAT AAT CAG AGG TG
S135	CCT GAT TGA AAG AAA TTG CGT AGA CCC GAA CG
S136	ATC AAA ATC GTC GCT ATT AAT TAA CGG ATT CG
S137	ACG CTC AAA ATA AGA ATA AAC ACC GTG AAT TT
S138	GGT ATT AAG AAC AAG AAA AAT AAT TAA AGC CA
S139	ATT ATT TAA CCC AGC TAC AAT TTT CAA GAA CG
S140	GAA GGA AAA TAA GAG CAA GAA ACA ACA GCC AT
S141	GAC TTG AGA GAC AAA AGG GCG ACA AGT TAC CA
S142	GCC ACC ACT CTT TTC ATA ATC AAA CCG TCA CC
S143	CTG AAA CAG GTA ATA AGT TTT AAC CCC TCA GA
S144	CTC AGA GCC ACC ACC CTC ATT TTC CTA TTA TT

S145	CCG CCA GCC ATT GCA ACA GGA AAA ATA TTT TT
S146	GAA TGG CTA GTA TTA ACA CCG CCT CAA CTA AT
S147	AGA TTA GAT TTA AAA GTT TGA GTA CAC GTA AA
S148	ACA GAA ATC TTT GAA TAC CAA GTT CCT TGC TT
S149	CTG TAA ATC ATA GGT CTG AGA GAC GAT AAA TA
S150	AGG CGT TAC AGT AGG GCT TAA TTG ACA ATA GA
S151	TAA GTC CTA CCA AGT ACC GCA CTC TTA GTT GC
S152	TAT TTT GCT CCC AAT CCA AAT AAG TGA GTT AA
S153	GCC CAA TAC CGA GGA AAC GCA ATA GGT TTA CC
S154	AGC GCC AAC CAT TTG GGA ATT AGA TTA TTA GC
S155	GTT TGC CAC CTC AGA GCC GCC ACC GAT ACA GG
S156	AGT GTA CTT GAA AGT ATT AAG AGG CCG CCA CC
S157	GCC ACG CTA TAC GTG GCA CAG ACA ACG CTC AT
S158	ATT TTG CGT CTT TAG GAG CAC TAA GCA ACA GT
S159	GCG CAG AGA TAT CAA AAT TAT TTG ACA TTA TC
S160	TAA CCT CCA TAT GTG AGT GAA TAA ACA AAA TC
S161	CAT ATT TAG AAA TAC CGA CCG TGT TAC CTT TT
S162	CAA GCA AGA CGC GCC TGT TTA TCA AGA ATC GC
S163	TTT TGT TTA AGC CTT AAA TCA AGA ATC GAG AA
S164	ATA CCC AAG ATA ACC CAC AAG AAT AAA CGA TT
S165	AAT CAC CAA ATA GAA AAT TCA TAT ATA ACG GA
S166	CAC CAG AGT TCG GTC ATA GCC CCC GCC AGC AA
S167	CCT CAA GAA TAC ATG GCT TTT GAT AGA ACC AC

S168	CCC TCA GAA CCG CCA CCC TCA GAA CTG AGA CT
S169	GGA AAT ACC TAC ATT TTG ACG CTC ACC TGA AA
S170	GCG TAA GAG AGA GCC AGC AGC AAA AAG GTT AT
S171	CTA AAA TAG AAC AAA GAA ACC ACC AGG GTT AG
S172	AAC CTA CCG CGA ATT ATT CAT TTC CAG TAC AT
S173	AAA TCA ATG GCT TAG GTT GGG TTA CTA AAT TT
S174	AAT GGT TTA CAA CGC CAA CAT GTA GTT CAG CT
S175	AAT GCA GAC CGT TTT TAT TTT CAT CTT GCG GG
S176	AGG TTT TGA ACG TCA AAA ATG AAA GCG CTA AT
S177	ATC AGA GAA AGA ACT GGC ATG ATT TTA TTT TG
S178	TCA CAA TCG TAG CAC CAT TAC CAT CGT TTT CA
S179	TCG GCA TTC CGC CGC CAG CAT TGA CGT TCC AG
S180	TAA GCG TCG AAG GAT TAG GAT TAG TAC CGC CA
S181	CTA AAG CAA GAT AGA ACC CTT CTG AAT CGT CT
S182	CGG AAT TAT TGA AAG GAA TTG AGG TGA AAA AT
S183	GAG CAA AAA CTT CTG AAT AAT GGA AGA AGG AG
S184	TAT GTA AAC CTT TTT TAA TGG AAA AAT TAC CT
S185	AGA GGC ATA ATT TCA TCT TCT GAC TAT AAC TA
S186	TCA TTA CCC GAC AAT AAA CAA CAT ATT TAG GC
S187	CTT TAC AGT TAG CGA ACC TCC CGA CGT AGG AA
S188	TTA TTA CGG TCA GAG GGT AAT TGA ATA GCA GC
S189	CCG GAA ACA CAC CAC GGA ATA AGT AAG ACT CC
S190	TGA GGC AGG CGT CAG ACT GTA GCG TAG CAA GG

S191	TGC TCA GTC AGT CTC TGA ATT TAC CAG GAG GT
S192	TAT CAC CGT ACT CAG GAG GTT TAG CGG GGT TT
S193	GAA ATG GAT TAT TTA CAT TGG CAG ACA TTC TG
S194	GCC AAC AGT CAC CTT GCT GAA CCT GTT GGC AA
S195	ATC AAC AGT CAT CAT ATT CCT GAT TGA TTG TT
S196	TGG ATT ATG AAG ATG ATG AAA CAA AAT TTC AT
S197	TTG AAT TAT GCT GAT GCA AAT CCA CAA ATA TA
S198	TTT TAG TTT TTC GAG CCA GTA ATA AAT TCT GT
S199	CCA GAC GAG CGC CCA ATA GCA AGC AAG AAC GC
S200	GAG GCG TTA GAG AAT AAC ATA AAA GAA CAC CC
S201	TGA ACA AAC AGT ATG TTA GCA AAC TAA AAG AA
S202	ACG CAA AGG TCA CCA ATG AAA CCA ATC AAG TT
S203	TGC CTT TAG TCA GAC GAT TGG CCT GCC AGA AT
S204	GGA AAG CGA CCA GGC GGA TAA GTG AAT AGG TG

Table 3-2. Staple strands with 5-T passivation extension at the 5' end.

Staple	Sequence (5’ – 3’)
5t1	TTT TTC GAT GGC CCA CTA CGT AAA CCG TC
5t2	TTT TTC GGT TTG CGT ATT GGG AAC GCG CG
5t5	TTT TTG ATG AAC GGT AAT CGT AGC AAA CA
5t6	TTT TTG GTT GTA CCA AAA ACA AGC ATA AA
5t7	TTT TTC TGT AGC TCA ACA TGT ATT GCT GA
5t8	TTT TTC ATT GAA TCC CCC TCA AAT CGT CA
5t11	TTT TTG ACA GCA TCG GAA CGA ACC CTC AG
5t12	TTT TTA CTT TCA ACA GTT TCT GGG ATT TT
5t205	TTT TTA CCA GTA ATA AAA GGG ATT CAC CA
5t206	TTT TTA ATC AAT ATC TGG TCA CAA ATA TC
5t209	TTT TTC GCG AGA AAA CTT TTT ATC GCA AG
5t210	TTT TTC GAC AAA AGG TAA AGT AGA GAA TA
5t211	TTT TTG CTT ATC CGG TAT TCT AAA TCA GA
5t212	TTT TTG ACG GGA GAA TTA ACT ACA GGG AA
5t215	TTT TTA TAA ATC CTC ATT AAA TGA TAT TC
5t216	TTT TTT ATA AGT ATA GCC CGG CCG TCG AG
5t205	TTT TTA CCA GTA ATA AAA GGG ATT CAC CA
5t206	TTT TTA ATC AAT ATC TGG TCA CAA ATA TC

Table 3-3. Capture strand sequences for loading aptamer TBA15.

Staple	Sequence (5' – 3')
27-A	AAA AAA AAA AAA AAA GCC AGC TGC CTG CAG GTC GAC TCT GCA AGG CG
29-A	AAA AAA AAA AAA AAA ACC CGT CGT CAT ATG TAC CCC GGT AAA GGC TA
31-A	AAA AAA AAA AAA AAA CAA AAT TAA AGT ACG GTG TCT GGA AGA GGT CA
33-A	AAA AAA AAA AAA AAA ACT GGA TAA CGG AAC AAC ATT ATT ACC TTA TG
35-A	AAA AAA AAA AAA AAA GCT CCA TGA GAG GCT TTG AGG ACT AGG GAG TT

Table 3-4. Capture strand sequences for loading aptamer TBA29

Staple	Sequence (5’ – 3’)
38-AT	ATA ATA ATA ATA ATA CCC GGG TAC TTT CCA GTC GGG AAA CGG GCA AC
40-AT	ATA ATA ATA ATA ATA AGA AAA GCA ACA TTA AAT GTG AGC ATC TGC CA
42-AT	ATA ATA ATA ATA ATA TCC ATA TAC ATA CAG GCA AGG CAA CTT TAT TT
44-AT	ATA ATA ATA ATA ATA AAA GAT TCA GGG GGT AAT AGT AAA CCA TAA AT
46-AT	ATA ATA ATA ATA ATA TTT CAT GAA AAT TGT GTC GAA ATC TGT ACA GA

References

(1) Dey, S.; Fan, C.; Gothelf, K. V.; Li, J.; Lin, C.; Liu, L.; Liu, N.; Nijenhuis, M. A. D.; Saccà, B.; Simmel, F. C.; Yan, H.; Zhan, P. DNA Origami. *Nat. Rev. Methods Prim. 2021 11* **2021**, *1* (1), 1–24.

(2) Seeman, N. C. Nucleic Acid Junctions and Lattices. *J. Theor. Biol.* **1982**, *99* (2), 237–247.

(3) Seeman, N. C.; Belcher, A. M. Emulating Biology: Building Nanostructures from the Bottom Up. *Proc. Natl. Acad. Sci.* **2002**, *99* (suppl 2), 6451–6455.

(4) Seeman, N. C.; Sleiman, H. F. DNA Nanotechnology. *Nat. Rev. Mater. 2017 31* **2017**, *3* (1), 1–23.

(5) Baig, N.; Kammakakam, I.; Falath, W.; Kammakakam, I. Nanomaterials: A Review of Synthesis Methods, Properties, Recent Progress, and Challenges. *Mater. Adv.* **2021**, *2* (6), 1821–1871.

(6) Seeman, N. C. In the Nick of Space: Generalized Nucleic Acid Complementarity and DNA Nanotechnology. *Synlett* **2000**, No. 11, 1536–1548.

(7) Goodnow, R. A. J. Just Enough Knowledge... In *A handbook for DNA-encoded chemistry : theory and applications for exploring chemical space and drug discovery*; John Wiley & Sons, Inc., 2014; pp 2–16.

(8) Watson, J. D.; Crick, F. H. C. Molecular Structure of Nucleic Acids: A Structure for Deoxyribose Nucleic Acid. *Nat. 1953 1714356* **1953**, *171* (4356), 737–738.

(9) Spencer, M. The Stereochemistry of Deoxyribonucleic Acid. II. Hydrogen-Bonded Pairs of Bases. *Aeta Cryst* **1959**, *12*, 66.

(10) LaBean, T. H.; Yan, H.; Kopatsch, J.; Liu, F.; Winfree, E.; Reif, J. H.; Seeman, N.

C. Construction, Analysis, Ligation, and Self-Assembly of DNA Triple Crossover Complexes. *J. Am. Chem. Soc.* **2000**, *122* (9), 1848–1860.

(11) Winfree, E.; Liu, F.; Wenzler, L. A.; Seeman, N. C. Design and Self-Assembly of Two-Dimensional DNA Crystals. *Nat. 1998 3946693* **1998**, *394* (6693), 539–544.

(12) Seeman, N. C. From Genes to Machines: DNA Nanomechanical Devices. *Trends Biochem. Sci.* **2005**, *30* (3), 119–125.

(13) McBride, L. J.; Caruthers, M. H. An Investigation of Several Deoxynucleoside Phosphoramidites Useful for Synthesizing Deoxyoligonucleotides. *Tetrahedron Lett.* **1983**, *24* (3), 245–248.

(14) Hamblin, G. D.; Rahbani, J. F.; Sleiman, H. F. Sequential Growth of Long DNA Strands with User-Defined Patterns for Nanostructures and Scaffolds. *Nat. Commun. 2015 61* **2015**, *6* (1), 1–8.

(15) Lau, K. L.; Sleiman, H. F. Minimalist Approach to Complexity: Templating the Assembly of DNA Tile Structures with Sequentially Grown Input Strands. *ACS Nano* **2016**, *10* (7), 6542–6551.

(16) He, Y.; Tian, Y.; Chen, Y.; Deng, Z.; Ribbe, A. E.; Mao, C.; He, Y.; Tian, Y.; Chen, Y.; Deng, Z.; Ribbe, A. E.; Mao, C. Sequence Symmetry as a Tool for Designing DNA Nanostructures. *Angew. Chemie Int. Ed.* **2005**, *44* (41), 6694–6696.

(17) Shih, W. M.; Quispe, J. D.; Joyce, G. F. A 1.7-Kilobase Single-Stranded DNA That Folds into a Nanoscale Octahedron. *Nat. 2004 4276975* **2004**, *427* (6975), 618–621.

(18) Rothemund, P. W. K. Folding DNA to Create Nanoscale Shapes and Patterns. *Nat.*

2006 4407082 **2006**, *440* (7082), 297–302.

(19) Zhao, S.; Tian, R.; Wu, J.; Liu, S.; Wang, Y.; Wen, M.; Shang, Y.; Liu, Q.; Li, Y.; Guo, Y.; Wang, Z.; Wang, T.; Zhao, Y.; Zhao, H.; Cao, H.; Su, Y.; Sun, J.; Jiang, Q.; Ding, B. A DNA Origami-Based Aptamer Nanoarray for Potent and Reversible Anticoagulation in Hemodialysis. *Nat. Commun.* **2021**, *12* (1), 1–10.

(20) Castro, C. E.; Kilchherr, F.; Kim, D. N.; Shiao, E. L.; Wauer, T.; Wortmann, P.; Bathe, M.; Dietz, H. A Primer to Scaffolded DNA Origami. *Nat. Methods 2011 83* **2011**, *8* (3), 221–229.

(21) Tapio, K.; Bald, I. The Potential of DNA Origami to Build Multifunctional Materials. *Multifunct. Mater.* **2020**, *3* (3), 032001.

(22) Kopielski, A.; Schneider, A.; Csáki, A.; Fritzsche, W. Isothermal DNA Origami Folding: Avoiding Denaturing Conditions for One-Pot, Hybrid-Component Annealing. *Nanoscale* **2015**, *7* (5), 2102–2106.

(23) Chandrasekaran, A. R.; Pushpanathan, M.; Halvorsen, K. Evolution of DNA Origami Scaffolds. *Mater. Lett.* **2016**, *170*, 221–224.

(24) Zhang, F.; Jiang, S.; Wu, S.; Li, Y.; Mao, C.; Liu, Y.; Yan, H. Complex Wireframe DNA Origami Nanostructures with Multi-Arm Junction Vertices. *Nat. Nanotechnol.* **2015**, *10* (9), 779–784.

(25) Platnich, C. M.; Hariri, A. A.; Sleiman, H. F.; Cosa, G. Advancing Wireframe DNA Nanostructures Using Single-Molecule Fluorescence Microscopy Techniques. *Acc. Chem. Res.* **2019**.

(26) Platnich, C. M.; Hariri, A. A.; Rahbani, J. F.; Gordon, J. B.; Sleiman, H. F.; Cosa, G. Kinetics of Strand Displacement and Hybridization on Wireframe DNA

Nanostructures: Dissecting the Roles of Size, Morphology, and Rigidity. *ACS Nano* **2018**, *12* (12), 12836–12846.

(27) Douglas, S. M.; Marblestone, A. H.; Teerapittayanon, S.; Vazquez, A.; Church, G. M.; Shih, W. M. Rapid Prototyping of 3D DNA-Origami Shapes with CaDNAno. *Nucleic Acids Res.* **2009**, *37* (15), 5001.

(28) Kim, D. N.; Kilchherr, F.; Dietz, H.; Bathe, M. Quantitative Prediction of 3D Solution Shape and Flexibility of Nucleic Acid Nanostructures. *Nucleic Acids Res.* **2012**, *40* (7), 2862–2868.

(29) Pan, K.; Kim, D. N.; Zhang, F.; Adendorff, M. R.; Yan, H.; Bathe, M. Lattice-Free Prediction of Three-Dimensional Structure of Programmed DNA Assemblies. *Nat. Commun. 2014 51* **2014**, *5* (1), 1–7.

(30) Wohlert, J.; Den Otter, W. K.; Edholm, O.; Briels, W. J. Free Energy of a Trans-Membrane Pore Calculated from Atomistic Molecular Dynamics Simulations. *J. Chem. Phys.* **2006**, *124* (15), 154905.

(31) Rothemund, P. W. K. Folding DNA to Create Nanoscale Shapes and Patterns Supplementary Notes 1-11.

(32) Jun, H.; Wang, X.; Bricker, W. P.; Bathe, M. Automated Sequence Design of 2D Wireframe DNA Origami with Honeycomb Edges. *Nat. Commun. 2019 101* **2019**, *10* (1), 1–9.

(33) Jun, H.; Shepherd, T. R.; Zhang, K.; Bricker, W. P.; Li, S.; Chiu, W.; Bathe, M. Automated Sequence Design of 3D Polyhedral Wireframe DNA Origami with Honeycomb Edges. *ACS Nano* **2019**, *13* (2), 2083–2093.

(34) Benson, E.; Mohammed, A.; Bosco, A.; Teixeira, A. I.; Orponen, P.; Högberg, B.

Computer-Aided Production of Scaffolded DNA Nanostructures from Flat Sheet Meshes. *Angew. Chemie - Int. Ed.* **2016**, *55* (31), 8869–8872.

(35) Jun, H.; Zhang, F.; Shepherd, T.; Ratanalert, S.; Qi, X.; Yan, H.; Bathe, M. Autonomously Designed Free-Form 2D DNA Origami. *Sci. Adv.* **2019**, *5* (1).

(36) Kekic, T.; Barisic, I. In Silico Modelling of DNA Nanostructures. *Comput. Struct. Biotechnol. J.* **2020**, *18*, 1191.

(37) Veneziano, R.; Ratanalert, S.; Zhang, K.; Zhang, F.; Yan, H.; Chiu, W.; Bathe, M. Designer Nanoscale DNA Assemblies Programmed from the Top Down. *Science* **2016**, *352* (6293), 1534.

(38) De Llano, E.; Miao, H.; Ahmadi, Y.; Wilson, A. J.; Beeby, M.; Viola, I.; Barisic, I. Adenita: Interactive 3D Modelling and Visualization of DNA Nanostructures. *Nucleic Acids Res.* **2020**, *48* (15), 8269–8275.

(39) Miao, H.; De Llano, E.; Sorger, J.; Ahmadi, Y.; Kekic, T.; Isenberg, T.; Gröller, M. E.; Barišić, I.; Viola, I. Multiscale Visualization and Scale-Adaptive Modification of DNA Nanostructures. *IEEE Trans. Vis. Comput. Graph.* **2018**, *24* (1), 1014–1024.

(40) Andersen, E. S.; Dong, M.; Nielsen, M. M.; Jahn, K.; Lind-Thomsen, A.; Mamdouh, W.; Gothelf, K. V.; Besenbacher, F.; Kjems, J. DNA Origami Design of Dolphin-Shaped Structures with Flexible Tails. *ACS Nano* **2008**, *2* (6), 1213–1218.

(41) Kuzuya, A.; Komiyama, M. Design and Construction of a Box-Shaped 3D-DNA Origami. *Chem. Commun.* **2009**, No. 28, 4182–4184.

(42) Zhang, Q.; Jiang, Q.; Li, N.; Dai, L.; Liu, Q.; Song, L.; Wang, J.; Li, Y.; Tian, J.;

Ding, B.; Du, Y. DNA Origami as an in Vivo Drug Delivery Vehicle for Cancer Therapy. *ACS Nano* **2014**, *8* (7), 6633–6643.

(43) Sun, W.; Boulais, E.; Hakobyan, Y.; Wang, W. L.; Guan, A.; Bathe, M.; Yin, P. Casting Inorganic Structures with DNA Molds. *Science (80-.).* **2014**, *346* (6210), 6210.

(44) Jiang, Q.; Song, C.; Nangreave, J.; Liu, X.; Lin, L.; Qiu, D.; Wang, Z. G.; Zou, G.; Liang, X.; Yan, H.; Ding, B. DNA Origami as a Carrier for Circumvention of Drug Resistance. *J. Am. Chem. Soc.* **2012**, *134* (32), 13396–13403.

(45) Kumar, N.; Seminario, J. M. Molecular Dynamics Study of Thrombin Capture by Aptamers TBA26 and TBA29 Coupled to a DNA Origami. *https://doi.org/10.1080/08927022.2018.1448977* **2018**, *44* (9), 749–756.

(46) Mayer, G.; Mayer, G. The Chemical Biology of Aptamers. *Angew. Chemie Int. Ed.* **2009**, *48* (15), 2672–2689.

(47) Mairal, T.; Cengiz Özalp, V.; Lozano Sánchez, P.; Mir, M.; Katakis, I.; O'Sullivan, C. K. Aptamers: Molecular Tools for Analytical Applications. *Anal. Bioanal. Chem.* **2008**, *390* (4), 989–1007.

(48) Beaucage, S. L.; Iyer, R. P. Advances in the Synthesis of Oligonucleotides by the Phosphoramidite Approach. *Tetrahedron* **1992**, *48* (12), 2223–2311.

(49) Keefe, A. D.; Pai, S.; Ellington, A. Aptamers as Therapeutics. *Nat. Rev. Drug Discov.* **2010**, *9* (7), 537–550.

(50) Beaucage, S. L.; Iyer, R. P. The Synthesis of Modified Oligonucleotides by the Phosphoramidite Approach and Their Applications. *Tetrahedron* **1993**, *49* (28), 6123–6194.

(51) Baugh, C.; Grate, D.; Wilson, C. 2.8 Å Crystal Structure of the Malachite Green Aptamer. *J. Mol. Biol.* **2000**, *301* (1), 117–128.

(52) Baker, B. R.; Lai, R. Y.; Wood, M. S.; Doctor, E. H.; Heeger, A. J.; Plaxco, K. W. An Electronic, Aptamer-Based Small-Molecule Sensor for the Rapid, Label-Free Detection of Cocaine in Adulterated Samples and Biological Fluids. *J. Am. Chem. Soc.* **2006**, *128* (10), 3138–3139.

(53) Rangnekar, A.; Zhang, A. M.; Li, S. S.; Bompiani, K. M.; Hansen, M. N.; Gothelf, K. V.; Sullenger, B. A.; LaBean, T. H. Increased Anticoagulant Activity of Thrombin-Binding DNA Aptamers by Nanoscale Organization on DNA Nanostructures. *Nanomedicine Nanotechnology, Biol. Med.* **2012**, *8* (5), 673–681.

(54) Riccardi, C.; Napolitano, E.; Musumeci, D.; Montesarchio, D. Dimeric and Multimeric DNA Aptamers for Highly Effective Protein Recognition. *Mol. 2020,* **2020**, *25* (22), 5227.

(55) Jiang, Y.; Zhu, C.; Ling, L.; Wan, L.; Fang, X.; Bai, C. Specific Aptamer−Protein Interaction Studied by Atomic Force Microscopy. *Anal. Chem.* **2003**, *75* (9), 2112–2116.

(56) McKeague, M.; Derosa, M. C. Challenges and Opportunities for Small Molecule Aptamer Development. *J. Nucleic Acids* **2012**, *2012*, 20.

(57) Ruscito, A.; DeRosa, M. C. Small-Molecule Binding Aptamers: Selection Strategies, Characterization, and Applications. *Front. Chem.* **2016**, *4* (MAY), 14.

(58) Hassan, E. M.; Mohamed, A.; DeRosa, M. C.; Willmore, W. G.; Hanaoka, Y.; Kiwa, T.; Ozaki, T. High-Sensitivity Detection of Metastatic Breast Cancer Cells via Terahertz Chemical Microscopy Using Aptamers. *Sensors Actuators B Chem.*

2019, *287*, 595–601.

(59) Bock, L. C.; Griffin, L. C.; Latham, J. A.; Vermaas, E. H.; Toole, J. J. Selection of Single-Stranded DNA Molecules That Bind and Inhibit Human Thrombin. *Nat. 1992 3556360* **1992**, *355* (6360), 564–566.

(60) Tasset, D. M.; Kubik, M. F.; Steiner, W. Oligonucleotide Inhibitors of Human Thrombin That Bind Distinct Epitopes. *J. Mol. Biol.* **1997**, *272* (5), 688–698.

(61) Musumeci, D.; Montesarchio, D. Polyvalent Nucleic Acid Aptamers and Modulation of Their Activity: A Focus on the Thrombin Binding Aptamer. *Pharmacol. Ther.* **2012**, *136* (2), 202–215.

(62) Huntington, J. A. Molecular Recognition Mechanisms of Thrombin. *J. Thromb. Haemost.* **2005**, *3* (8), 1861–1872.

(63) Huntington, J. A.; Baglin, T. P. Targeting Thrombin – Rational Drug Design from Natural Mechanisms. *Trends Pharmacol. Sci.* **2003**, *24* (11), 589–595.

(64) Müller, J.; Wulffen, B.; Pötzsch, B.; Mayer, G. Multidomain Targeting Generates a High-Affinity Thrombin-Inhibiting Bivalent Aptamer. *ChemBioChem* **2007**, *8* (18), 2223–2226.

(65) Wlotzka, B.; Leva, S.; Eschgfäller, B.; Burmeister, J.; Kleinjung, F.; Kaduk, C.; Muhn, P.; Hess-Stumpp, H.; Klussmann, S. In Vivo Properties of an Anti-GnRH Spiegelmer: An Example of an Oligonucleotide-Based Therapeutic Substance Class. *Proc. Natl. Acad. Sci. U. S. A.* **2002**, *99* (13), 8898–8902.

(66) Hartwig, A. Role of Magnesium in Genomic Stability. *Mutat. Res. Mol. Mech. Mutagen.* **2001**, *475* (1–2), 113–121.

(67) Wagenbauer, K. F.; Engelhardt, F. A. S.; Stahl, E.; Hechtl, V. K.; Stömmer, P.;

Seebacher, F.; Meregalli, L.; Ketterer, P.; Gerling, T.; Dietz, H. How We Make DNA Origami. *ChemBioChem* **2017**, *18* (19), 1873–1885.

(68) Sobczak, J. P. J.; Martin, T. G.; Gerling, T.; Dietz, H. Rapid Folding of DNA into Nanoscale Shapes at Constant Temperature. *Science (80-.).* **2012**, *338* (6113), 1458–1461.

(69) Shaw, A.; Benson, E.; Högberg, B. Purification of Functionalized DNA Origami Nanostructures. *ACS Nano* **2015**, *9* (5), 4968–4975.

(70) Stahl, E.; Martin, T. G.; Praetorius, F.; Dietz, H. Facile and Scalable Preparation of Pure and Dense DNA Origami Solutions. *Angew. Chemie* **2014**, *126* (47), 12949–12954.

(71) Bellot, G.; McClintock, M. A.; Lin, C.; Shih, W. M. Recovery of Intact DNA Nanostructures after Agarose Gel-Based Separation. *Nat. Methods* **2011**, *8* (3), 192–194.

(72) Douglas, S. M.; Bachelet, I.; Church, G. M. A Logic-Gated Nanorobot for Targeted Transport of Molecular Payloads. *Science* **2012**, *335* (6070), 831–834.

(73) Thamm, S.; Slesiona, N.; Dathe, A.; Csáki, A.; Fritzsche, W. AFM-Based Probing of the Flexibility and Surface Attachment of Immobilized DNA Origami. *Langmuir* **2018**, *34* (49), 15093–15098.

(74) Bangalore, D. M.; Tessmer, I.; Bangalore, D. M.; Tessmer, I. Unique Insight into Protein-DNA Interactions from Single Molecule Atomic Force Microscopy. *AIMS Biophys. 2018 3194* **2018**, *5* (3), 194–216.

(75) Lyubchenko, Y. L.; Shlyakhtenko, L. S.; Ando, T. Imaging of Nucleic Acids with Atomic Force Microscopy. *Methods* **2011**, *54* (2), 274.

(76) Mei, Q.; Johnson, R. H.; Wei, X.; Su, F.; Liu, Y.; Kelbauskas, L.; Lindsay, S.; Meldrum, D. R.; Yan, H.; Berlin, S.-V. On-Chip Isotachophoresis Separation of Functional DNA Origami Capture Nanoarrays from Cell Lysate. *Nano Res.* **2013**, No. 6.

(77) Fan, S.; Wang, D.; Kenaan, A.; Cheng, J.; Cui, D.; Song, J. Create Nanoscale Patterns with DNA Origami. *Small* **2019**, *15* (26), 1805554.

(78) Ke, Y.; Lindsay, S.; Chang, Y.; Liu, Y.; Yan, H. Self-Assembled Water-Soluble Nucleic Acid Probe Tiles for Label-Free RNA Hybridization Assays. *Science* **2008**, *319* (5860), 180–183.

(79) Wang, X.; Lim, H. J.; Son, A. Characterization of Denaturation and Renaturation of DNA for DNA Hybridization. *Environ. Health Toxicol.* **2014**, *29*, e2014007.

(80) Chao, J.; Zhang, H.; Xing, Y.; Li, Q.; Liu, H.; Wang, L.; Wang, L.; Fan, C. Programming DNA Origami Assembly for Shape-Resolved Nanomechanical Imaging Labels. *Nat. Protoc. 13*.

(81) Zhu, B.; Zhao, Y.; Dai, J.; Wang, J.; Xing, S.; Guo, L.; Chen, N.; Qu, X.; Li, L.; Shen, J.; Shi, J.; Li, J.; Wang, L. Preservation of DNA Nanostructure Carriers: Effects of Freeze-Thawing and Ionic Strength during Lyophilization and Storage. *ACS Appl. Mater. Interfaces* **2017**, *9* (22), 18434–18439.

(82) Kim, H.; Surwade, S. P.; Powell, A.; O'Donnell, C.; Liu, H. Stability of DNA Origami Nanostructure under Diverse Chemical Environments. *Chem. Mater.* **2014**, *26* (18), 5265–5273.

(83) Kielar, C.; Xin, Y.; Xu, X.; Zhu, S.; Gorin, N.; Grundmeier, G.; Möser, C.; Smith, D. M.; Keller, A. Effect of Staple Age on DNA Origami Nanostructure Assembly

and Stability. *Molecules* **2019**, *24* (14).

(84) An, R.; Jia, Y.; Wan, B.; Zhang, Y.; Dong, P.; Li, J.; Liang, X. Non-Enzymatic Depurination of Nucleic Acids: Factors and Mechanisms. *PLoS One* **2014**, *9* (12), e115950.

(85) Song, J.; Arbona, J. M.; Zhang, Z.; Liu, L.; Xie, E.; Elezgaray, J.; Aime, J. P.; Gothelf, K. V.; Besenbacher, F.; Dong, M. Direct Visualization of Transient Thermal Response of a DNA Origami. *J. Am. Chem. Soc.* **2012**, *134* (24), 9844–9847.

(86) Nwokeoji, A. O.; Kilby, P. M.; Portwood, D. E.; Dickman, M. J. Accurate Quantification of Nucleic Acids Using Hypochromicity Measurements in Conjunction with UV Spectrophotometry. *Anal. Chem.* **2017**, *89* (24), 13567–13574.

(87) Mahler, H. R.; Kline, B.; Mehrotra, B. D. Some Observations on the Hypochromism of DNA. *J. Mol. Biol.* **1964**, *9* (3), 801–811.

(88) Gao, Y.; Wolf, L. K.; Georgiadis, R. M. Secondary Structure Effects on DNA Hybridization Kinetics: A Solution versus Surface Comparison. *Nucleic Acids Res.* **2006**, *34* (11), 3370.

(89) Lutter, L.; Serpell, C. J.; Tuite, M. F.; Serpell, L. C.; Xue, W. F. Three-Dimensional Reconstruction of Individual Helical Nano-Filament Structures from Atomic Force Microscopy Topographs. *Biomol. Concepts* **2020**, *11* (1), 102–115.

(90) Ramakrishnan, S.; Krainer, G.; Grundmeier, G.; Schlierf, M.; Keller, A. Structural Stability of DNA Origami Nanostructures in the Presence of Chaotropic Agents. *Nanoscale* **2016**, *8* (19), 10398–10405.

(91) McConnell, E. M.; Bolzon, R.; Mezin, P.; Frahm, G.; Johnston, M.; DeRosa, M. C. PHAST (PH-Driven Aptamer Switch for Thrombin) Catch-and-Release of Target Protein. *Bioconjug. Chem.* **2016**, *27* (6), 1493–1499.